Phase and frequency shifts in a population of phase oscillators

Peter Tass
Department of Neurology, Heinrich-Heine-University, Moorenstrasse 5, D-40225 Düsseldorf, Germany
(Received 23 October 1996; revised manuscript received 29 April 1997)

We investigate the synchronization behavior of a population of globally coupled phase oscillators with randomly distributed eigenfrequencies. A variety of synchronized states is rigorously analyzed by means of the center manifold theorem combined with a nonlinear renormalization procedure. This way, the different synchronized states are determined explicitly. We observe n-cluster states, where $n=1,\ldots,4$. In a synchronized state all oscillators have the same frequency. Synchronization frequency and mutual phase differences depend on model parameters as well as on the configuration of the synchronized state, i.e., the number of oscillators within each cluster. The synchronization frequency may decisively differ from the mean of the eigenfrequencies, e.g., giving rise to *frozen states*, which are synchronized states with vanishing synchronization frequency. Unstable cluster states are associated with transitions between different synchronization frequencies. Our approach can easily be extended to a population of oscillators with randomly distributed coupling strengths. The different synchronized states are discussed in the context of neural coding. [S1063-651X(97)03908-1]

PACS number(s): 87.10.+e, 05.45.+b

I. INTRODUCTION

During the act of perception sensory segmentation separates the sensory input into pieces which form patterns. For instance, in order to recognize single objects of the visual world, the brain has to separate different objects from each other and from the background. This process is called scene segmentation or figure-ground segregation [1,2]. The neurophysiological mechanism which realizes scene segmentation is still a matter of debate. It is well known that local visual features are detected by single neurons with suitable receptive field properties [3,11]. An object consisting of several local features can only be recognized if the local information is combined appropriately [1,2]. It was suggested that this process is realized by means of a temporal neuronal firing code [2,4,5]. In particular, von der Malsburg and Schneider suggested that sensory segmentation is realized by an in-phase synchronization of the firing activity of all neurons encoding local features which belong to one particular object [5]. This notion was confirmed as synchronized oscillatory neuronal activity was found in rabbit [6], cat [7,8,12], pigeon [9], and monkey [10].

A multitude of theoretical studies dedicated to the dynamics of populations of oscillators showed that apart from in-phase synchronization and incoherent activity there is a variety of qualitatively different dynamical phenomena, for instance, splay-phase states [13], attractor crowding [14], plateaus of frequency-locked oscillators [15,16], clustering [17–21], dephasing and bursting [22], finite-size-induced transitions [23], and collective chaotic behavior [19,24,25]. Thus from a theoretical point of view one might expect that apart from synchrony of periodic activity and incoherency the experimental data might display other dynamical states which cannot be detected by means of the typically applied linear correlation techniques. Nevertheless, these dynamical states might play an important role as far as the neuronal code and in particular sensory segmentation is concerned.

In order to decide which dynamical states might be interesting in the context of the neuronal code, we take into account that neurons are coincidence detectors (see, e.g., [5]). For this reason we are interested in synchronized states exhibiting groups of mutually synchronized oscillators as is well known from the so-called cluster states [17–21].

Let us recall that there are different levels of synchronization. (a) Synchrony (in-phase synchronization) is the strongest form of synchronization, where the phase difference between any two oscillators vanishes (modulo 2π). (b) A weaker form of synchronization is phase locking, where the oscillators' mutual phase differences are constant, but generally do not vanish. (c) The term frequency locking denotes a synchronized state in which all oscillators have the same average frequency, whereas there need not be a fixed phase relationship. (d) Clustering is a more local type of synchronization typically investigated in lattices of oscillators with local interactions [17]. Anyhow, clustering occurs in populations of globally coupled oscillators, too [18–21]. Due to the mutual interactions the oscillators form several clusters. Within each cluster all oscillators have the same phase. The phase differences between different clusters do not vanish; generally they are functions in time. A state is called cluster state if the number of different clusters remains finite as $N\to\infty$, where N is the number of oscillators.

In this study we investigate a population of globally coupled phase oscillators with continuous interactions. Depending on the model parameters and the system's initial conditions all oscillators may form one giant cluster or they may break into two, three, or four phase-locked clusters of arbitrary size. The phase difference between any two oscillators within one cluster vanishes or is small as compared with the phase difference between different clusters (cf. Fig. 1). The cluster states under consideration are phase-locked states in which all oscillators run at the same frequency, i.e., $\dot{\psi}_j=\Omega^*$ for $j=1,\ldots,N$, where ψ_j is the phase of the jth oscillator, N is the number of all oscillators, and Ω^* is the synchronization frequency. Synchronization frequency and shifts of the mutual phase differences decisively depend on the number of oscillators within each cluster.

Note that we do not intend to present a detailed model for

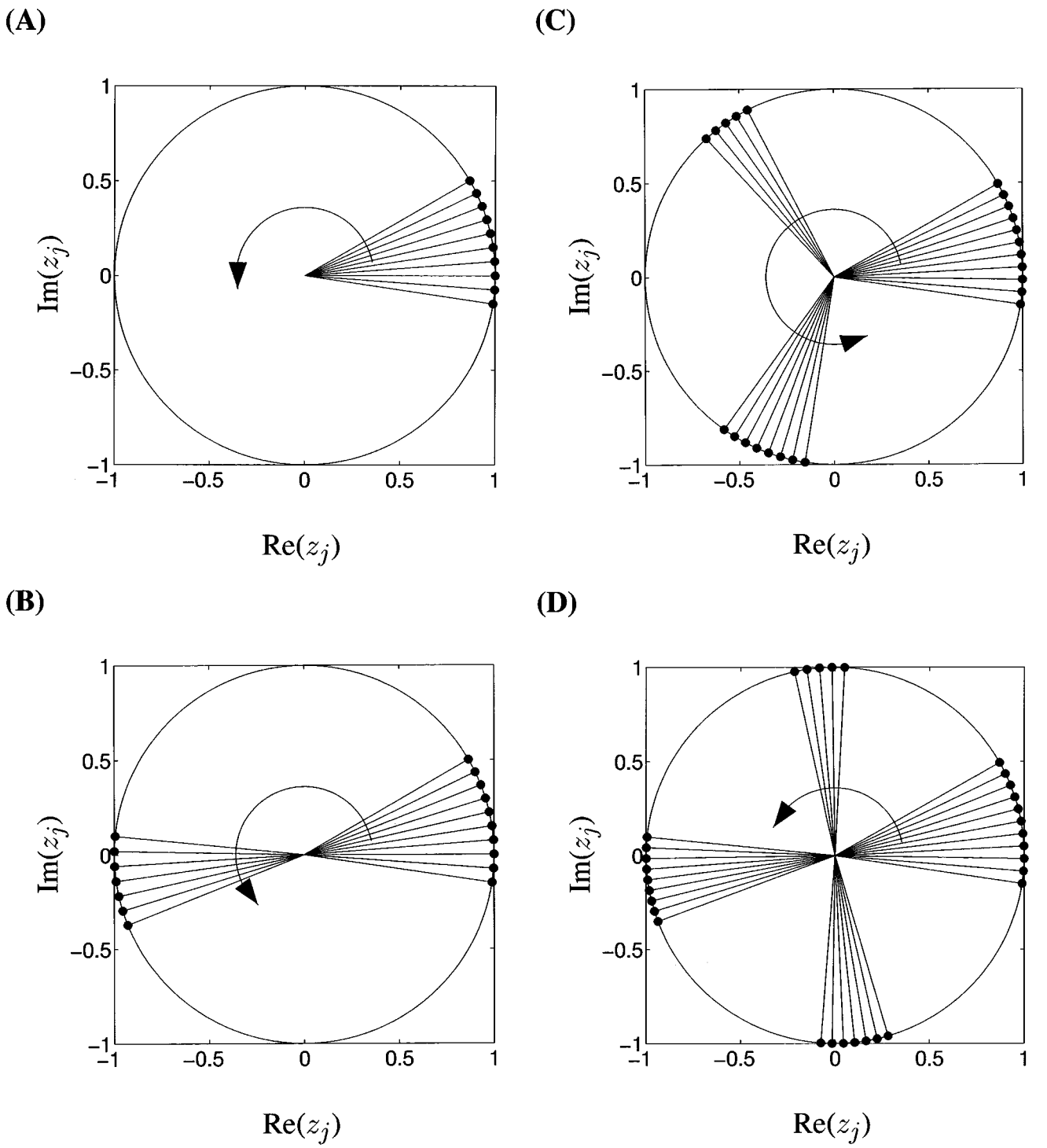

FIG. 1. *Schematic illustration of the different synchronized states*: A single oscillator is represented by a dot (connected with the origin) on the unit circle in the complex plane according to $z_j = \exp(i\psi_j)$. A synchronized state consists of one (A), two (B), three (C), or four (D) clusters in each of which the oscillators have constant small (or vanishing) mutual phase differences. All oscillators run at the same frequency. The latter depends on the model parameters as well as on the synchronization configuration, i.e., the number of oscillators within the different clusters. Different configurations are typically associated with different synchronization frequencies as indicated by arrows of different length. The synchronized states will be called the one-cluster state (A), two-cluster state (B), three-cluster state (C), four-cluster state (D).

synchronized neuronal activity in the visual cortex as was done in other studies [26–28]. The model analyzed in the present article may be augmented to become a minimal model for synchronized neuronal activity in the visual cortex, e.g., along the lines of a previous study [28]. However, our main concern in this paper is to investigate synchronization phenomena which are interesting from both the theoretical and the neurophysiological point of view. In particular, we analyze the relationship between synchronization frequency and locking behavior in a population of phase oscil-

lators. From the physiological standpoint interest in this relationship rose as a consequence of recent experimental findings. For instance, it was observed that the activation of the mesencephalic reticular formation caused an enhancement of stimulus-specific synchronization associated with an increase of the synchronization frequency [29].

The paper is organized as follows. In Sec. II we introduce the model equation. Section III is devoted to the analytical investigation of the different cluster states under consideration. Numerical results are presented in Sec. IV. In Sec. V we sketch how the model equation can be augmented to become a minimal model of synchronized neuronal activity in the visual cortex. Finally in Sec. VI we summarize and discuss our results.

II. THE MODEL EQUATION

Winfree proposed to approximate the dynamics of a population of limit cycle oscillators by means of the dynamics of a population of phase oscillators [30]. He assumed that the coupling is weak as compared with the attractiveness of the limit cycle. Thus the coupling predominately affects the motion of each oscillator around its limit cycle. Kuramoto provided a sound mathematical framework for this notion of phase oscillators in the case of weak coupling [31]. As far as phase and frequency shifts in the synchronized states are concerned this approximation also holds in the case of strong coupling for different networks of limit cycle oscillators [33].

A typical model equation for smoothly interacting phase oscillators reads [30,31]

$$\dot{\psi}_j=\omega_j-\sum_{k=1}^{N}\Gamma_{jk}(\psi_j-\psi_k)\quad(j=1,\ldots,N),\tag{1}$$

where ψ_j is the phase of the jth oscillator, and ω_j is the eigenfrequency of the jth oscillator. The oscillators' mutual interactions are modeled by Γ_{jk}, where $\Gamma_{jk}(x+2\pi)=\Gamma_{jk}(x)$ holds. Thus we can expand Γ_{jk} in terms of Fourier modes. In the case of globally coupled oscillators we are allowed to set $\Gamma_{jk}(x)=\Gamma(x)$. If one is interested in interactions giving rise to in-phase synchronization it is sufficient to take into account first order terms of $\Gamma(x)$, for instance, $\Gamma(x)=KN^{-1}\sin(x)$, where K is the coupling strength (cf. [31]). Higher harmonics of the coupling Γ enrich the dynamical behavior of Eq. (1) considerably: Aside from macroscopic synchronization [32] one encounters clustering [20,21]. For this reason we take into account Fourier modes up to fourth order, this way obtaining our model equation

$$\dot{\psi}_j=\omega_j-\frac{1}{N}\sum_{k=1}^{N}\sum_{m=1}^{4}\{K_m\sin[m(\psi_j-\psi_k)]+C_m\cos[m(\psi_j-\psi_k)]\},\tag{2}$$

where we assume that $K_m>0$ holds. Before we turn to our analytical analysis let us first introduce several notations. Mean and variance of all eigenfrequencies will be denoted by $\Omega=N^{-1}\Sigma_{k=1}^{N}\omega_k$ and $V=N^{-1}\Sigma_{x=1}^{N}(\omega_k-\Omega)^2$. By means of deviations η_k the eigenfrequencies may be written as $\omega_k=\Omega+\eta_k$. In the synchronized states analyzed below all oscillators have the same frequency, which will be called *synchronization frequency*. As a consequence of mutual phase differences one up to four clusters of synchronized oscillators evolve (cf. Fig. 1). The *cluster frequency* of the νth cluster, i.e., the mean of the eigenfrequencies of the oscillators in the νth cluster, will be denoted by $\Omega_\nu=N_\nu^{-1}\Sigma_{k(\nu)}\omega_k$, where $\Sigma_{k(\nu)}$ denotes summation over all k, where the kth oscillator is in the νth cluster. N_ν denotes the number of oscillators in the νth cluster. Deviations of the cluster frequencies Λ_ν are introduced by setting $\Omega_\nu=\Omega+\Lambda_\nu$. The variance of the eigenfrequencies of the νth cluster reads $V_\nu=N_\nu^{-1}\Sigma_{k(\nu)}(\omega_k-\Omega_\nu)^2=N_\nu^{-1}\Sigma_{k(\nu)}(\eta_k-\Lambda_\nu)^2$. The third moment of the distribution of all eigenfrequencies will be denoted by $M=N^{-1}\Sigma_{k=1}^{N}(\omega_k-\Omega)^3=N^{-1}\Sigma_{k=1}^{N}\eta_k^3$. Finally we introduce the term *configuration of the synchronized state* which will be defined by the number of oscillators within each cluster, no matter which particular oscillator belongs to a certain cluster. In this article we briefly denote the configuration of the synchronized state as *configuration*. Let us, for example, consider the three-cluster state [Fig. 1(C)]. In this case the configuration is given by (N_1,N_2,N_3).

III. ANALYTICAL INVESTIGATION

Below it will turn out that the model equation (2) displays a rich synchronization behavior. Aside from synchrony the population of oscillators may break into two, three, or four phase-locked clusters as illustrated in Fig. 1. The different synchronized states have to be analyzed separately. However, our strategy remains the same in all four cases. Therefore in the following section we briefly sketch the strategy. Our investigation essentially relies on the center manifold theorem [34]. In Sec. III B we explain how to apply this theorem along the lines of our approach. Next we investigate the different synchronized states in Secs. III C–III F.

A. Strategy

Let us briefly sketch the main features of our analysis.

(1) We introduce a rotating coordinate system. Due to a suitable choice of the rotation frequency in the rotating coordinate system the synchronized state under consideration is nothing but a stable fixed point. The proper rotation frequency is the synchronization frequency denoted by Ω^*.

(2) The system's dynamics acts on two time scales, where the slow variables determine the motion of the fast variables as is well known from the slaving principle [35,36]. In particular, in all synchronized states the slow variables are constant. For this reason it is convenient to determine phase and frequency shifts explicitly by means of the center manifold theorem [34]. Moreover the center manifold theorem enables us to prove the stability of the different synchronized states.

(3) The center manifold theorem can only be applied if the coordinate system is rotating with a suitable frequency. A renormalization procedure guarantees that the proper rotation frequency is chosen. In oscillator theory renormalization by linear counterterms is a common tool for the determination of frequency shifts caused by the coupling [36]. In previous

studies a combination of linear renormalization and center manifold theorem was used in order to analyze phase and frequency shifts in some oscillator models [33,37]. However, as far as model equation (2) is concerned a linear renormalization procedure will not work. This will be discussed in Sec. III C. For this reason in the present paper we perform a *nonlinear renormalization procedure*.

B. Center manifold

It is our goal to determine the synchronized states explicitly. To this end in Secs. III C–III F we perform suitable transformations which cast model equation (2) into a form which allows us to apply the center manifold theorem effectively. These transformations are different in the four cases. As a result of these transformations the state of the population of oscillators is described by two sets of variables: the center modes and the stable modes. Denoting the vectors of the center and the stable modes by $\mathbf{x}_c$ and $\mathbf{x}_s$, the transformed system reads

$$\dot{\mathbf{x}}_c = B_c \mathbf{x}_c + \mathbf{n}_c(\mathbf{x}_c, \mathbf{x}_s), \tag{3}$$

$$\dot{\mathbf{x}}_s = B_s \mathbf{x}_s + \mathbf{n}_s(\mathbf{x}_c, \mathbf{x}_s). \tag{4}$$

The eigenvalues of the matrix B_c vanish, whereas the eigenvalues of the matrix B_s have negative real parts. $\mathbf{n}_c(\mathbf{x}_c, \mathbf{x}_s)$ and $\mathbf{n}_s(\mathbf{x}_c, \mathbf{x}_s)$ denote the nonlinear terms. As a consequence of the above mentioned transformations the linear parts of the stable modes and the center modes are separated from each other. Neglecting nonlinear terms in Eqs. (3) and (4) we obtain the Jordan form of the linear problem (cf. [38], Chap. 6). In a small neighborhood of zero the stable modes are given by the center modes according to

$$\mathbf{x}_s = \mathbf{h}(\mathbf{x}_c), \tag{5}$$

where $\mathbf{h}$ only contains terms of second and higher order [34]. Equation (5) characterizes the center manifold. The parameter range in which Eq. (5) is valid will be stated more precisely below. On the center manifold the dynamics obeys $\dot{\mathbf{x}}_c = B_c \mathbf{x}_c + \mathbf{n}_c(\mathbf{x}_c, \mathbf{h}(\mathbf{x}_c))$ [34]. This equation is the so-called reduced problem. Thus in order to analyze the dynamics on the center manifold we have to determine $\mathbf{h}$. To this end we differentiate Eq. (5) with respect to time, obtaining $\dot{\mathbf{x}}_s = D\mathbf{h}(\mathbf{x}_c)\dot{\mathbf{x}}_c$, where D denotes the differentiation operator. With Eqs. (3) and (4) we immediately see that

$$B_s \mathbf{h}(\mathbf{x}_c) + \mathbf{n}_s(\mathbf{x}_c, \mathbf{h}(\mathbf{x}_c)) = D\mathbf{h}(\mathbf{x}_c)[B_c \mathbf{x}_c + \mathbf{n}_c(\mathbf{x}_c, \mathbf{h}(\mathbf{x}_c))] \tag{6}$$

has to be fulfilled. Obviously the determination of $\mathbf{h}$ may be rather complicated. Additionally the resulting reduced problem may be so complex that it would be impossible to carry out an analytic investigation. Hence we perform a *nonlinear renormalization procedure* as explained in Sec. III C. As a result of this procedure $B_c \mathbf{x}_c$ as well as $\mathbf{n}_c(\mathbf{x}_c, \mathbf{h}(\mathbf{x}_c))$ vanish on the center manifold. This way our analysis is decisively simplified. (a) The reduced problem becomes trivial as it reads $\dot{\mathbf{x}}_c = \mathbf{0}$. (b) On the other hand, Eq. (6) takes the simple form

$$\mathbf{h}(\mathbf{x}_c) = -B_s^{-1} \mathbf{n}_s(\mathbf{x}_c, \mathbf{h}(\mathbf{x}_c)). \tag{7}$$

Anyhow, it may still be impossible or at least complicated to invert the matrix B_s analytically. For this reason (a) we (rigorously) introduce an additional variable, and (b) we assume that some of the coupling constants obey certain smallness conditions. As a consequence of these manipulations the matrix of the stable part of the transformed model equation is given by

$$B_s = -\gamma E, \tag{8}$$

where E denotes the identity matrix, and γ is a positive constant. Inserting Eq. (8) into Eq. (7) we end up with

$$\mathbf{h}(\mathbf{x}_c) = \frac{1}{\gamma} \mathbf{n}_s(\mathbf{x}_c, \mathbf{h}(\mathbf{x}_c)), \tag{9}$$

which enables us to determine terms of lowest order of $\mathbf{h}$ in a straightforward way. According to the center manifold theorem the states described by Eq. (5) are stable because they are local attractors [34]. Equation (5) determines a *stable fixed point* because the reduced problem reads $\dot{\mathbf{x}}_c = \mathbf{0}$. As a result of the above mentioned suitable transformations the fixed point is nothing but the synchronized state under consideration. Note that the center manifold theorem only holds if

$$\|\mathbf{x}_c\| \ll \gamma \tag{10}$$

is fulfilled (cf. [34]). Due to this condition the deviations $\eta_1, \ldots, \eta_N$ and some of the coupling constants have to be small as compared with γ. This will be discussed in detail below. For larger values of $\|\mathbf{x}_c\|$ we have to analyze the synchronized states, for instance, numerically.

C. One cluster

In this section we analyze a synchronized state given by one cluster of oscillators all having the same frequency and small mutual phase differences [cf. Fig. 1(A)]. To this end we introduce *relative phases*

$$\phi_j(t) = \psi_j(t) - \Omega^* t - \theta. \tag{11}$$

θ is a constant phase shift which will be determined below. Ω^* is the *synchronization frequency*, i.e., the oscillators' frequency in the synchronized state, given by

$$\Omega^* = \Omega - \Delta, \tag{12}$$

with Ω as introduced in Sec. II. Δ is a *counterterm* which is expanded in terms of ε, where $0 < \varepsilon \ll 1$ holds:

$$\Delta=\sum_{\nu=0}^{\infty}\Delta^{(\nu)}\varepsilon^{\nu}. \tag{13}$$

Δ will contribute to a *nonlinear renormalization* of the eigenfrequencies. To this end $\Delta^{(0)},\Delta^{(1)},\Delta^{(2)},\ldots$ will be chosen appropriately below. Inserting Eq. (11) into the model equation (2) we obtain

$$\dot{\phi}_j=\eta_j+\Delta-\frac{1}{N}\sum_{k=1}^{N}\sum_{m=1}^{4}\{K_m\sin[m(\phi_j-\phi_k)] + C_m\cos[m(\phi_j-\phi_k)]\}. \tag{14}$$

Moreover we introduce the abbreviations

$$a=\sum_{m=1}^{4} m\ K_m, \quad b=\frac{1}{2}\sum_{m=1}^{4} m^2\ C_m, \quad c=\frac{1}{6}\sum_{m=1}^{4} m^3\ K_m. \tag{15}$$

On the other hand, we introduce an additional variable by setting

$$\rho(t)=\frac{1}{N}\sum_{k=1}^{N}\phi_k(t). \tag{16}$$

This (rigorous) trick decisively simplifies our analysis, which is based on the center manifold theorem. In particular, the matrix of the stable modes (B_s) is simply a diagonal matrix which can be inverted in a straightforward way [cf. Eq. (8)].

ε as well as $\eta_1,\ldots,\eta_N$ are constant. Thus we can (rigorously) treat them as variables which do not change: $\dot{\varepsilon}=\dot{\eta}_1=\cdots=\dot{\eta}_N=0$. Therefore $\varepsilon,\eta_1,\ldots,\eta_N$ are center modes (cf. Sec. III B). We want to cast Eq. (3) into a most convenient form. For this reason we postulate that

$$\dot{\rho}=0 \quad \text{on the center manifold} \tag{17}$$

has to be fulfilled. This can easily be achieved by an appropriate choice of the counterterms $\Delta^{(0)},\Delta^{(1)},\Delta^{(2)},\ldots$ from Eq. (13). As a consequence of condition (17), Eq. (3) simply reads $\dot{\mathbf{x}}_c=\mathbf{0}$. If condition (17) is fulfilled, the synchronized state is a stable fixed point which lies within a small neighborhood around zero as will be shown below. Therefore by means of the center manifold theorem we can calculate the fixed point explicitly in order to determine phase and frequency shifts. On the other hand, if condition (17) is not fulfilled we obtain $\dot{\rho}=M(\varepsilon,\eta_1,\ldots,\eta_N)$, where M does not depend on ρ. Thus $\rho(t)=Mt+\rho_0$ ($\rho_0=\text{const}$). In this case ρ increases or decreases monotonously. Consequently the system does not stay within a small neighborhood around zero. Thus the center manifold cannot be applied. For this reason we have to guarantee that condition (17) is fulfilled by means of proper counterterms ($\Delta^{(0)},\Delta^{(1)},\Delta^{(2)},\ldots$). In particular, below it will turn out that for $C_j\neq 0$ condition (17) is not fulfilled if we perform a linear renormalization by merely fitting counterterms $\Delta^{(0)}$ and $\Delta^{(1)}$.

Of course, the center manifold is not yet determined. The determination of the counterterms is performed in several steps.

(a) The equations for $\dot{\phi}_1,\ldots,\dot{\phi}_N$ and condition (17) are expanded according to Taylor. $\Delta^{(0)},\Delta^{(1)}$ are determined by taking into account constant terms and terms of first order. In this article the order of terms refers to the center modes. Thus terms of nth order are $\sim\|\mathbf{x}_c\|^n$.

(b) In order to separate the linear parts of center and stable modes we perform the transformation $\varphi_j=\phi_j-\eta_j/a-\rho$ so that the vectors of center and stable modes are given by $\mathbf{x}_c=(\varepsilon,\rho,\eta_1,\ldots,\eta_N)^T$, $\mathbf{x}_s=(\varphi_1,\ldots,\varphi_N)^T$. $(\cdots)^T$ denotes the transposed vector $(\cdots)$. As a result of this transformation the matrix of the stable modes is of the form presented by Eq. (8), where $\gamma=a$ [cf. Eq. (15)].

(c) $\mathbf{h}$ is determined in lowest order according to Eq. (9).

(d) In order to determine counterterms of higher order, i.e., $\Delta^{(2)},\Delta^{(3)},\ \Delta^{(4)},\ldots$, we insert $\mathbf{h}$ into condition (17), this way taking into account nonlinear terms. The determination of these counterterms is in principle trivial. Nevertheless, it is quite tedious. Thus in this study we restrict ourselves to the determination of frequency shifts of second order, i.e., $\Delta^{(2)}$. Note that this *nonlinear renormalization* is only possible because we treat ε as variable.

We immediately see that condition (17) is *always* fulfilled (not only on the center manifold) if $C_1=C_2=C_3=C_4=0$. In this case ρ is a *conserved quantity*, no matter whether the system is synchronized or not, and correspondingly Δ vanishes. But if at least one of the coefficients C_1,C_2,C_3,C_4 does not vanish, we have to choose the counterterms $\Delta^{(0)},\Delta^{(1)},\Delta^{(2)},\ldots$ appropriately so that condition (17) is fulfilled. This yields

$$\Delta^{(0)}=\sum_{m=1}^{4} C_m, \quad \Delta^{(1)}=0, \quad \Delta^{(2)}=-\frac{2b}{\varepsilon^2 a^2}V. \tag{18}$$

These counterterms describe the frequency shifts, which occur in the synchronized state as a result of the oscillators' mutual interactions. We still have to calculate the phase shifts $\phi_1,\ldots,\phi_N$ in the synchronized state [cf. Eq. (11)]. The stable modes in the synchronized state are determined by the center modes according to Eq. (5): $\varphi_j=h_j(\mathbf{x}_c)$, where $\mathbf{h}(\mathbf{x}_c)=(h_1(\mathbf{x}_c),\ldots,h_N(\mathbf{x}_c))$. Taking into account that ρ vanishes on the center manifold for a suitable choice of $\theta=N^{-1}\Sigma_{k=1}{}^{N}\psi_k(0)$ with Eq. (11) we finally end up with the synchronized state

$$\psi_j(t)=\Omega^* t+\psi_j^{\text{stat}}, \quad \text{where} \quad \psi_j^{\text{stat}}=\theta+\frac{\eta_j}{a}+\chi_j \tag{19}$$

is a constant phase shift, and $\chi_j=\eta_j a^{-1}+h_j(\mathbf{x}_c)$. We obtain $\chi_j=(c\,\eta_j^3+3c\,\eta_j V-cM)/a^4+O(\|\mathbf{x}_c\|^4)$ if $C_1=\cdots=C_4=0$, or else we get $\chi_j=b(\eta_j^2-V)/a^3+O(\|\mathbf{x}_c\|^3)$. Thus in the synchronized state all oscillators have the same frequency,

$$\Omega^*=\Omega-\sum_{m=1}^{4} C_m+\frac{\sum_{m=1}^{4} m^2 C_m}{\left(\sum_{m=1}^{4} mK_m\right)^2}V+O(\|\mathbf{x}_c\|^3) \tag{20}$$

[cf. Eqs. (12), (13), and (18)], where V denotes the variance of the eigenfrequencies (cf. Sec. II). According to condition

(10) the deviations η_j have to be small in comparison with the coupling strength a [Eq. (15)]. Hence for randomly distributed $\eta_1, \ldots, \eta_N$ within the cluster we encounter small mutual phase differences, whereas for $\eta_1 = \cdots = \eta_N = 0$ all oscillators are perfectly synchronized, i.e., $\psi_j(t) = \psi(t)$ for $j = 1, \ldots, N$.

We already mentioned that as a consequence of condition (17) $\dot{\mathbf{x}}_c = \mathbf{0}$ holds. For this reason the center manifold is actually nothing but a point. On the other hand, the center manifold is a *local attractor* (cf. [34]). Thus the center manifold, i.e., the investigated synchronized state, is a stable fixed point.

D. Two clusters

We now analyze a synchronized state with two opposite clusters as shown in Fig. 1(B). N_ν denotes the number of oscillators in the νth cluster, and $N = N_1 + N_2$. Let us denote the normalized size of the νth cluster by $n_\nu = N_\nu / N$. For the two clusters we choose the ansatz $\phi_j(t) = \psi_j(t) - \Omega^* t - \theta - \vartheta_j$, where $\vartheta_j = 0$ for the oscillators of the first cluster (i.e., $j = 1, \ldots, N_1$) and $\vartheta_j = \pi$ for the oscillators of the second cluster (i.e., $j = N_1 + 1, \ldots, N$). In order to simplify our analysis, i.e., in order to apply the approach outlined in Sec. III B, we assume that $K_1, K_3, C_1, \ldots, C_4$ are small in comparison with the synchronizing coupling constants K_2 and K_4. For this reason we set $K_1 \to \varepsilon K_1$, $K_3 \to \varepsilon K_3$, $C_m \to \varepsilon C_m$, where $m = 1, \ldots, 4$. Note that ε is of the same order of magnitude as $\eta_1, \ldots, \eta_N$. This assumption guarantees that B_s is simply a diagonal matrix [cf. Eq. (8)] which can be inverted straightforwardly according to Eqs. (7) and (9).

As in the former section it is our goal to cast the system under consideration into the form given by Eqs. (3) and (4). To this end we perform the nonlinear renormalization, which guarantees that condition (17) is fulfilled. As a consequence of the proper choice of $\Delta^{(1)}$ we encounter new quantities, which will be denoted by

$$\eta_j^\dagger = \varepsilon (C_1 + C_3)[n_\mu - n_\nu + (n_\mu - n_\nu)^2], \tag{21}$$

where the jth oscillator is in the νth cluster, and $\mu \neq \nu$ (i.e., $\nu = 1, \mu = 2$ or $\nu = 2, \mu = 1$). These quantities cause a shift of the deviations $\eta_1, \ldots, \eta_N$. Hence we introduce

$$\xi_j = \eta_j + \eta_j^\dagger . \tag{22}$$

Moreover, we introduce *shifted eigenfrequencies* $\omega_j^\dagger$ by setting

$$\omega_j^\dagger = \omega_j + \eta_j^\dagger = \Omega + \eta_j + \eta_j^\dagger . \tag{23}$$

With Eq. (22) the transformation separating linear parts of center and stable modes reads $\varphi_j = \phi_j - \xi_j / (2K_2 + 4K_4) - \rho$. This transformation yields the vectors of the center and the stable modes:

$$\mathbf{x}_c = (\varepsilon, \rho, \xi_1, \ldots, \xi_N)^T, \quad \mathbf{x}_s = (\varphi_1, \ldots, \varphi_N)^T. \tag{24}$$

In comparison with the case of one synchronized cluster two synchronized clusters are associated with shifted deviations ξ_j serving as center modes. Taking into account condition (17) the frequency shift Δ is derived as explained in Sec. III C. This way, we obtain

$$\Delta^{(0)} = \Delta^{(2)} = 0, \quad \Delta^{(1)} = C_2 + C_4 + (C_1 + C_3)(n_1 - n_2)^2, \tag{25}$$

$$\Delta^{(3)} = \delta_{(3)} + \delta_{(3)}^\dagger , \tag{26}$$

with $\delta_{(3)}$ and $\delta_{(3)}^\dagger$ as in Eqs. (A1) and (A2). All quantities depending on $\eta_1^\dagger, \ldots, \eta_N^\dagger$ (such as $\delta_{(3)}^\dagger$) are indicated by the dagger. These quantities only depend on the configuration. In contrast to this the corresponding quantities without dagger (such as $\delta_{(3)}$) additionally depend on the eigenfrequency distribution (i.e., on $\{\eta_j\}$).

In order to determine the phase shifts we proceed as explained in Sec. III C, where in this case $\gamma = 2K_2 + 4K_4$. We now choose $\theta = (1/N) \sum_{k=1}^N \psi_k(0) - n_2 \pi$ so that ρ vanishes on the center manifold. Finally we end up with the stable synchronized state given by

$$\psi_j(t) = \Omega^* t + \psi_j^{\text{stat}}, \quad \text{where} \quad \psi_j^{\text{stat}} = \theta + \chi_j + \chi_j^\dagger + \vartheta_j \tag{27}$$

is the constant phase shift of the jth oscillator, where χ_j and $\chi_j^\dagger$, the shifts of higher order, are listed in Appendix A [Eqs. (A6) and (A7)]. χ_j gives rise to mutual phase differences within a single cluster. As a consequence of condition (10) the mutual phase differences are small in comparison with the coupling strength $(2K_2 + 4K_4)$. For $\eta_1 = \cdots = \eta_N = 0$ the oscillators within a single cluster are perfectly synchronized. On the other hand, $\chi_j^\dagger$ causes a systematic phase shift of a whole cluster, thereby disturbing the opposite arrangement of the two clusters determined by ϑ_j according to Eq. (27) (cf. Fig. 1). This deformation of the clusters' opposite arrangement will be illustrated numerically in Sec. IV A.

From Eqs. (12), (13), (25), and (26) we read off that for nonvanishing coupling constants $C_1, \ldots, C_4$ the synchronization frequency decisively depends on the configuration of the synchronized state, i.e., the number of oscillators within each cluster.

E. Three clusters

This section is devoted to a synchronized state with three equally spaced clusters [cf. Fig. 1(C)]. B_s, the matrix of the stable modes, is a simple diagonal matrix as in Eq. (8) if we assume that $K_\nu \to \varepsilon K_\nu$, $C_m \to \varepsilon C_m$ holds for $\nu = 1,2,4$ and $m = 1, \ldots, 4$. N_ν denotes the number of oscillators in the νth cluster, where $\nu = 1,2,3$, and $N = N_1 + N_2 + N_3$. In analogy to the former sections we choose the ansatz $\phi_j(t) = \psi_j(t) - \Omega^* t - \theta - \vartheta_j$, where $\vartheta_j = 0$ for the oscillators of the first cluster (i.e., $j = 1, \ldots, N_1$) and $\vartheta_j = 2\pi/3$ for the oscillators of the second cluster (i.e., $j = N_1 + 1, \ldots, N_1 + N_2$), and $\vartheta_j = 4\pi/3$ for the oscillators of the third cluster (i.e., $j = N_1 + N_2 + 1, \ldots, N$). As in the former section due to the renormalization, in particular as a consequence of the proper choice of $\Delta^{(1)}$, we have to introduce shifts of the eigenfrequencies [Eq. (B3) in Appendix B] according to Eq. (23). With ξ_j from Eq. (22) linear parts of center and stable modes are separated by the transformation $\varphi_j = \phi_j - \xi_j / (3K_3) - \rho$ providing us with $\mathbf{x}_c$ and $\mathbf{x}_s$ given by

Eq. (24). Based on condition (17) the frequency shift Δ is derived as in the former section. This way, we end up with

$$\Delta^{(1)}=C_3+\frac{1}{2}(C_1+C_2+C_4)[(n_1-n_2)^2+(n_2-n_3)^2 + (n_3-n_1)^2], \tag{28}$$

$$\Delta^{(0)}=0, \quad \Delta^{(2)}=\delta_{(2)}+\delta_{(2)}^{\dagger}, \tag{29}$$

where $\delta_{(2)}$ and $\delta_{(2)}^{\dagger}$ are listed in Appendix B [Eqs. (B4) and (B5)]. The phase shifts are determined in a similar way as in the former sections. With $\gamma=3K_3$ we immediately obtain $h_j(\mathbf{x}_c)=H_j(\mathbf{x}_c)+H_j^{\dagger}(\mathbf{x}_c)$ according to Eq. (9). $H_j(\mathbf{x}_c)$ and $H_j^{\dagger}(\mathbf{x}_c)$ are presented in Appendix B. ρ vanishes on the center manifold if $\theta=N^{-1}\Sigma_{k=1}^{N}\psi_k(0)-(n_2+2n_3)2\pi/3$. Transforming back to the phases we obtain the stable synchronized state:

$$\psi_j(t)=\Omega^* t+\psi_j^{\mathrm{stat}},$$

$$\psi_j^{\mathrm{stat}}=\theta+\vartheta_j+\frac{\eta_j+\eta_j^{\dagger}}{3K_3}+H_j(\mathbf{x}_c)+H_j^{\dagger}(\mathbf{x}_c), \tag{30}$$

with $H_j(\mathbf{x}_c)$ and $H_j^{\dagger}(\mathbf{x}_c)$ from Eqs. (B1) and (B2). Δ, η_j, $\eta_j^{\dagger}$, H_j, and $H_j^{\dagger}$ have to be small in comparison with the coupling strength $\gamma=3K_3$ due to condition (10). If this condition is not fulfilled our approach is no longer valid, and we have to restrict ourselves to a numerical investigation, which is presented in Sec. IV.

So, Eq. (30) describes a synchronized state, where all oscillators have the same frequency Ω^* which deviates from the mean of the eigenfrequencies Ω according to Eqs. (12), (13), (28), and (B4). For nonvanishing coupling constants $C_1,\ldots,C_4$ the synchronization frequency crucially depends on the configuration of the synchronized state given by n_1,n_2,n_3. In the synchronized state we encounter three clusters consisting of N_1, N_2, and N_3 oscillators. Within a single cluster the oscillators display small mutual phase differences given by Eq. (30). The equal spacing of the clusters is disturbed if $H_j^{\dagger}$ and $\eta_j^{\dagger}$ do not vanish. In particular, clusters of equal size are equally spaced.

F. Four clusters

In this section we investigate four synchronized clusters which are equally spaced [cf. Fig. 1(D)]. Therefore we choose the ansatz $\phi_j(t)=\psi_j(t)-\Omega^* t-\theta-\vartheta_j$, where $\vartheta_j=0$ for the first cluster (i.e., $j=1,\ldots,N_1$), $\vartheta_j=\pi/2$ for the second cluster (i.e., $j=N_1+1,\ldots,N_1+N_2$), $\vartheta_j=\pi$ for the third cluster (i.e., $j=N_1+N_2+1,\ldots,N_1+N_2+N_3$), and $\vartheta_j=3\pi/2$ for the fourth cluster (i.e., $j=N_1+N_2+N_3+1,\ldots,N$). As usual N_ν denotes the number of oscillators in the νth cluster, and $N=N_1+N_2+N_3+N_4$. In order to achieve that B_s is of the form given by Eq. (8), we have to assume that $K_\nu\to\varepsilon K_\nu$ ($\nu=1,2,3$), $C_m\to\varepsilon C_m$ ($m=1,\ldots,4$) holds. As in Secs. III D and III E, due to the determination of $\Delta^{(1)}$ we have to introduce shifts of the eigenfrequencies [Eq. (C1) in Appendix C]. Separation of linear parts of center and stable modes is performed by the transformation $\varphi_j=\phi_j-\xi_j/4K_4-\rho$ with ξ_j from Eq. (22). This way, we obtain $\mathbf{x}_c$ and $\mathbf{x}_s$ given by Eq. (24). Based on condition (17) the frequency shift Δ is derived as in the former sections. With some calculations we arrive at

$$\Delta^{(0)}=0,$$

$$\Delta^{(1)}=C_4+C_2(n_1+n_3-n_2-n_4)^2 + (C_1+C_3)[(n_1-n_3)^2+(n_2-n_4)^2],$$

$$\Delta^{(2)}=\delta_{(2)}+\delta_{(2)}^{\dagger}, \tag{31}$$

where $\delta_{(2)}$ and $\delta_{(2)}^{\dagger}$ are listed in Appendix C [Eqs. (C2) and (C3)]. In order to derive the phase shifts we first determine $h_j(\mathbf{x}_c)=H_j(\mathbf{x}_c)+H_j^{\dagger}(\mathbf{x}_c)$ by means of Eq. (9) with $\gamma=4K_4$, where $H_j(\mathbf{x}_c)$ and $H_j^{\dagger}(\mathbf{x}_c)$ are listed in Appendix C. ρ vanishes on the center manifold for $\theta=(1/N)\Sigma_{k=1}^{N}\psi_k(0)-(n_2+2n_3+3n_4)\pi/2$. Finally we obtain the stable synchronized state

$$\psi_j(t)=\Omega^* t+\psi_j^{\mathrm{stat}},$$

$$\psi_j^{\mathrm{stat}}=\theta+\vartheta_j+\frac{\eta_j+\eta_j^{\dagger}}{4K_4}+H_j(\mathbf{x}_c)+H_j^{\dagger}(\mathbf{x}_c) \tag{32}$$

as constant phase shift, with $H_j(\mathbf{x}_c)$ and $H_j^{\dagger}(\mathbf{x}_c)$ from Appendix C. From condition (10) it follows that Δ, η_j, $\eta_j^{\dagger}$, H_j, and $H_j^{\dagger}$ are small in comparison with $\gamma=4K_4$.

Equation (30) describes a synchronized state, where all oscillators have the same frequency Ω^*. Ω^* critically depends on the configuration of the synchronized state $(n_1,\ldots,n_4)$. Within a single cluster the oscillators display small mutual phase differences due to χ_j, whereas $\chi_j^{\dagger}$ perturbs the clusters' equal spacing (cf. Fig. 1).

G. Hierarchy of frequency levels

For $\eta_1=\cdots=\eta_N=0$ our model displays a *multiplicity of attractors* (modulo 2π) which depends on the configuration: In the n-cluster state the attractors scale as

$$n_{\mathrm{comb}}(N_1,\ldots,N_n)=\frac{N!}{\Pi_{j=1}^{n}N_j!}, \quad \text{where} \quad N_1+\cdots+N_n=N. \tag{33}$$

In particular, if there is only one cluster all oscillators are in phase, and there is only one attractor. For randomly distributed $\eta_1,\ldots,\eta_N$ we observe small mutual phase differences according to Eq. (19) and a frequency shift of second order [cf. Eq. (20)].

On the other hand, if there are two or more clusters, a variety of frequency levels occurs, which depends on both the configuration and the eigenfrequency distribution. For the sake of clarity we introduce some notations. From Eqs. (25), (28), and (31) we immediately read off that $\Delta^{(1)}$ consists of two parts:

$$\Delta^{(1)}=\Delta_{\mathrm{I}}^{(1)}+\Delta_{\mathrm{II}}^{(1)}, \tag{34}$$

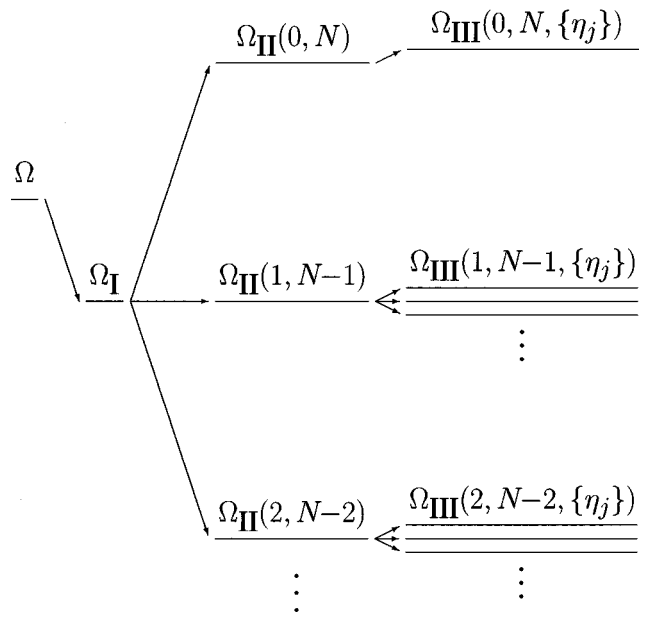

FIG. 2. *Hierarchy of frequency levels*: Schematic illustration of the different frequency levels corresponding to different configurations (N_1,N_2) of the two-cluster state. The frequency shift described by $\Omega_{\mathrm{I}}=\Omega-\Delta_{\mathrm{I}}^{(1)}\varepsilon$ is independent of the configuration as well as the eigenfrequency distribution. Lower order frequency splitting depends on the configuration $\Omega_{\mathrm{II}}(N_1,N_2)=\Omega-(\Delta_{\mathrm{I}}^{(1)}+\Delta_{\mathrm{II}}^{(1)})\varepsilon-\delta_{(3)}^{\dagger}\varepsilon^3$. The eigenfrequency distribution determines higher order frequency splitting according to $\Omega_{\mathrm{III}}(N_1,N_2,\{\eta_j\})=\Omega-(\Delta_{\mathrm{I}}^{(1)}+\Delta_{\mathrm{II}}^{(1)})\varepsilon-\delta_{(3)}^{\dagger}\varepsilon^3-\delta_{(3)}\varepsilon^3$. Note that frequency splitting only occurs in a synchronized state with more than one cluster.

where only $\Delta_{\mathrm{II}}^{(1)}$ depends on the configuration. With these notations we obtain for the n-cluster state $\Delta_{\mathrm{I}}^{(1)}=C_2+C_4$ $(n=2)$, $\Delta_{\mathrm{I}}^{(1)}=C_3 (n=3)$, and $\Delta_{\mathrm{I}}^{(1)}=C_4$ $(n=4)$. The configuration dependent shifts read $\Delta_{\mathrm{II}}^{(1)}=(C_1+C_3)(n_1-n_2)^2$ $(n=2)$, $\Delta_{\mathrm{II}}^{(1)}=(C_1+C_2+C_4)[(n_1-n_2)^2+(n_2-n_3)^2+(n_3-n_1)^2]/2$ $(n=3)$, and $\Delta_{\mathrm{II}}^{(1)}=C_2(n_1+n_3-n_2-n_4)+(C_1+C_3)[(n_1-n_3)^2+(n_2-n_4)^2]$ $(n=4)$. Obviously $\Delta_{\mathrm{II}}^{(1)}$ depends on asymmetries of the configuration.

In order to consider frequency shifts of lowest nonlinear order we take into account Eqs. (A1), (A2), (B4), (B5), (C2), and (C3). $\delta_{(2)}$ and $\delta_{(3)}$ depend on the eigenfrequency distribution $\{\eta_j\}$, whereas $\delta_{(2)}^{\dagger}$ and $\delta_{(3)}^{\dagger}$ only depend on the configuration. Thus for $n=2$ the synchronization frequency may be written as

$$\Omega_{\mathrm{III}}=\overbrace{\underbrace{\Omega-\Delta_{\mathrm{I}}^{(1)}\varepsilon}_{\Omega_{\mathrm{I}}}-\Delta_{\mathrm{II}}^{(1)}\varepsilon-\delta_{(3)}^{\dagger}\varepsilon^3}^{\Omega_{\mathrm{II}}}-\delta_{(3)}\varepsilon^3 \quad (35)$$

For $n=3,4$ we have to replace $\delta_{(3)}^{\dagger}\varepsilon^3$ and $\delta_{(3)}\varepsilon^3$ by $\delta_{(2)}^{\dagger}\varepsilon^2$ and $\delta_{(2)}\varepsilon^2$. The different terms of Eq. (35) find a clear interpretation as illustrated in Fig. 2.

(1) Ω_{I} takes into account frequency shifts of first order, which are independent of both configuration as well as eigenfrequency distribution.

(2) Ω_{II} summarizes frequency shifts of first and higher order, which exclusively depend on the configuration. Ω_{II} does not depend on the eigenfrequency distribution. As a consequence of the multiplicity of attractors as well as symmetry properties of Ω_{II} we encounter a *degeneracy of* Ω_{II}*-frequency levels* because every Ω_{II} level is associated with $n_{\mathrm{comb}}(N_1,\ldots,N_n)$ different synchronized states [cf. Eq. (33)]. This degeneracy is additionally increased due to symmetry properties of Ω_{II} [cf. Eqs. (34) and (35)]: Ω_{II} is invariant with respect to the interchange $N_j\leftrightarrow N_k$ $(n=2,3)$. In the four-cluster state Ω_{II} is invariant with respect to the interchange $N_2\leftrightarrow N_4$ for $N_1=N_3$ and $N_1\leftrightarrow N_3$ for $N_2=N_4$.

(3) Ω_{III} additionally takes into account terms of lowest nonlinear order ($\delta_{(3)}\varepsilon^3$ for $n=2$, $\delta_{(2)}\varepsilon^2$ for $n=3,4$) which depend on the eigenfrequency distribution $\{\eta_j\}$. For $\eta_1,\ldots,\eta_N\neq 0$, e.g., for randomly distributed $\{\omega_k\}$, every degenerated Ω_{II} level splits into a multitude of slightly different Ω_{III} levels [cf. Eqs. (A1), (B4), and (C2)].

IV. NUMERICAL INVESTIGATION

In this section we compare our analytical results with numerical simulations. Finally we discuss two phenomena, frozen states and characteristic transient behavior, which may be important, e.g., in the context of physiology.

A. Phase and frequency shifts

Two-cluster states are investigated numerically and analytically in this section, where $N=20$, $\eta_1=\cdots=\eta_N=0$, $K_2=0.5, K_1=K_3=K_4=0.01$. Due to $\eta_j=0$ all oscillators within one cluster share the same phase [modulo 2π, cf. Eq. (A6)]. Model equation (2) was integrated 19 times. In each simulation the system was started in the neighborhood of one of 19 different coexisting stable synchronized states with different synchronization configuration $(N_1=1,\ldots,19)$. In Figs. 3 and 4 we display the analytically derived *normalized phase difference* $\Delta\psi^{(1,2)}=(\psi_j^{\mathrm{stat}}-\psi_k^{\mathrm{stat}})/(2\pi)$ for two oscillators (j and k) from two different clusters with ψ_j^{stat} and ψ_k^{stat} from Eq. (27). $\Delta\psi^{(1)}$ takes into account terms of first order ($\sim\varepsilon$), whereas $\Delta\psi^{(2)}$ also takes into account terms of second order ($\sim\varepsilon^2$) [cf. Eq. (A7)]. Additionally in Figs. 3 and 4 we present $\Delta\psi^{\mathrm{num}}$, i.e., the numerically determined normalized phase difference between both clusters (performed by means of a fourth order Runge-Kutta algorithm).

While the oscillators within each cluster are perfectly synchronized, the phase difference between the two clusters depends on the configuration of the synchronized state (i.e., the number of oscillators within each cluster). We encounter an antiphase state ($\Delta\psi=0.5$) only if both clusters are of equal size ($n_1=n_2$). For $n_1\neq n_2$ the antiphase spacing is perturbed due to the quantities $\eta_1^{\dagger},\ldots,\eta_N^{\dagger}$, which cause a shift of the eigenfrequencies as explained in Sec. III D.

For the same simulations in Figs. 5 and 6 we plot the numerically determined mean synchronization frequency $\Omega_{\mathrm{num}}^{*}$ defined by $\Omega_{\mathrm{num}}^{*}=(\Sigma_{k=1}^{20}\omega_k^{*})/20$, where ω_k^{*} denotes the numerically determined synchronization frequency of the kth oscillator. Additionally in Figs. 5 and 6 we plot the analytically derived synchronization frequency, thereby taking into account terms of first order ($\Omega^{(1)}$) and also terms of

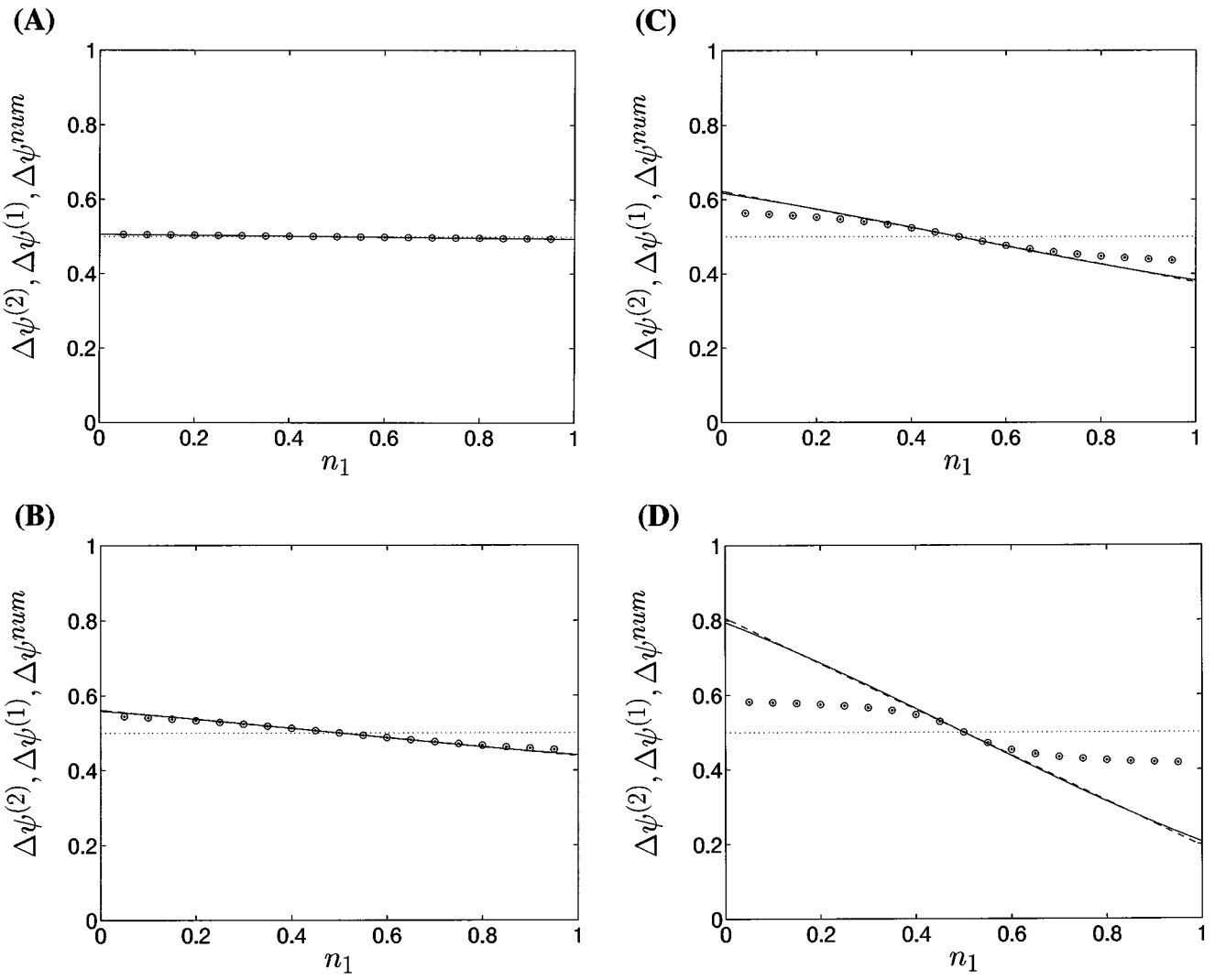

FIG. 3. *Normalized phase difference of two clusters*: Plots compare analytically derived and numerically revealed phase shifts in the synchronized states of two clusters, where $N=20$, $\eta_1=\cdots=\eta_N=0$, $K_2=0.5$, $K_1=K_3=K_4=0.01$. To this end $\Delta\psi^{\mathrm{num}}$ (dots, surrounded by small circles), $\Delta\psi^{(1)}$ (dashed line, covered by solid line), and $\Delta\psi^{(2)}$ (solid line) are determined and plotted according to the explanation in the text. Plots show normalized phase difference for different values of $C_1,\ldots,C_4$: $C_1=C_3=-0.01$, $C_2=C_4=0.01$ (A) [fulfilling smallness condition (10), i.e., $|C_j|\ll\gamma=2K_2+4K_4$], $C_1=C_3=-0.1$, $C_2=C_4=0.1$ (B), $C_1=C_3=-0.2$, $C_2=C_4=0.2$ (C), $C_1=C_3=-0.5$, $C_2=C_4=0.5$ (D). In order to illustrate differences between analytically derived and numerically revealed phase differences $\Delta\psi^{(1)}$ and $\Delta\psi^{(2)}$ are plotted as continuous functions of n_1.

third order ($\Omega^{(3)}$), where $\Omega^{(1)}=\Omega-\Delta^{(1)}\varepsilon$ and $\Omega^{(3)}=\Omega-\Delta^{(1)}\varepsilon-\Delta^{(3)}\varepsilon^3$ according to Eqs. (12), (13), (25), and (26).

If smallness condition (10) is fulfilled (justifying the application of the center manifold theorem) there is a perfect agreement between theoretical and numerical results [(A) in Figs. 3–6]. Even if the parameters $C_1,\ldots,C_4$ are of the same order of magnitude as the synchronizing coupling (K_2) there is a good agreement between theory and numerical results [(B) in Figs. 5 and 6]. For larger values of $C_1,\ldots,C_4$ terms of first and third order are no longer sufficient in order to achieve a good agreement between theory and simulation [(C) and (D) in Figs. 5 and 6]. In order to improve this agreement one has to derive higher order terms $\Delta^{(4)},\Delta^{(5)},\ldots$ along the lines of our approach. Nevertheless, for $|n_1-n_2|\ll 1$ as well as for $n_1=1$ or $n_2=1$ there is still a good agreement between analytical results and numerical results. $|K_1|$ and $|K_3|$ are small in comparison with $\gamma=2K_2+4K_4$. Therefore terms of second order contribute to $\Delta\psi$ only marginally [cf. Eq. (A7)]. Depending on the model parameters the synchronization frequency in the antiphase state may be larger or smaller as compared with the in-phase state.

B. Frozen states

In the former section we already showed that due to the oscillators' mutual interactions there may be dramatic shifts of the synchronization frequency. For this reason we suggest the term *frozen state* in order to denote a stable synchronized state with vanishing (or at most small) synchronization frequency. Plot (D) in Fig. 5 provides us with an example of a frozen state (for $n_1=0.5$). Two further examples are shown in Figs. 7 and 8.

The state of synchronization can conveniently be described in terms of collective variables [16,25,33,39]: ampli-

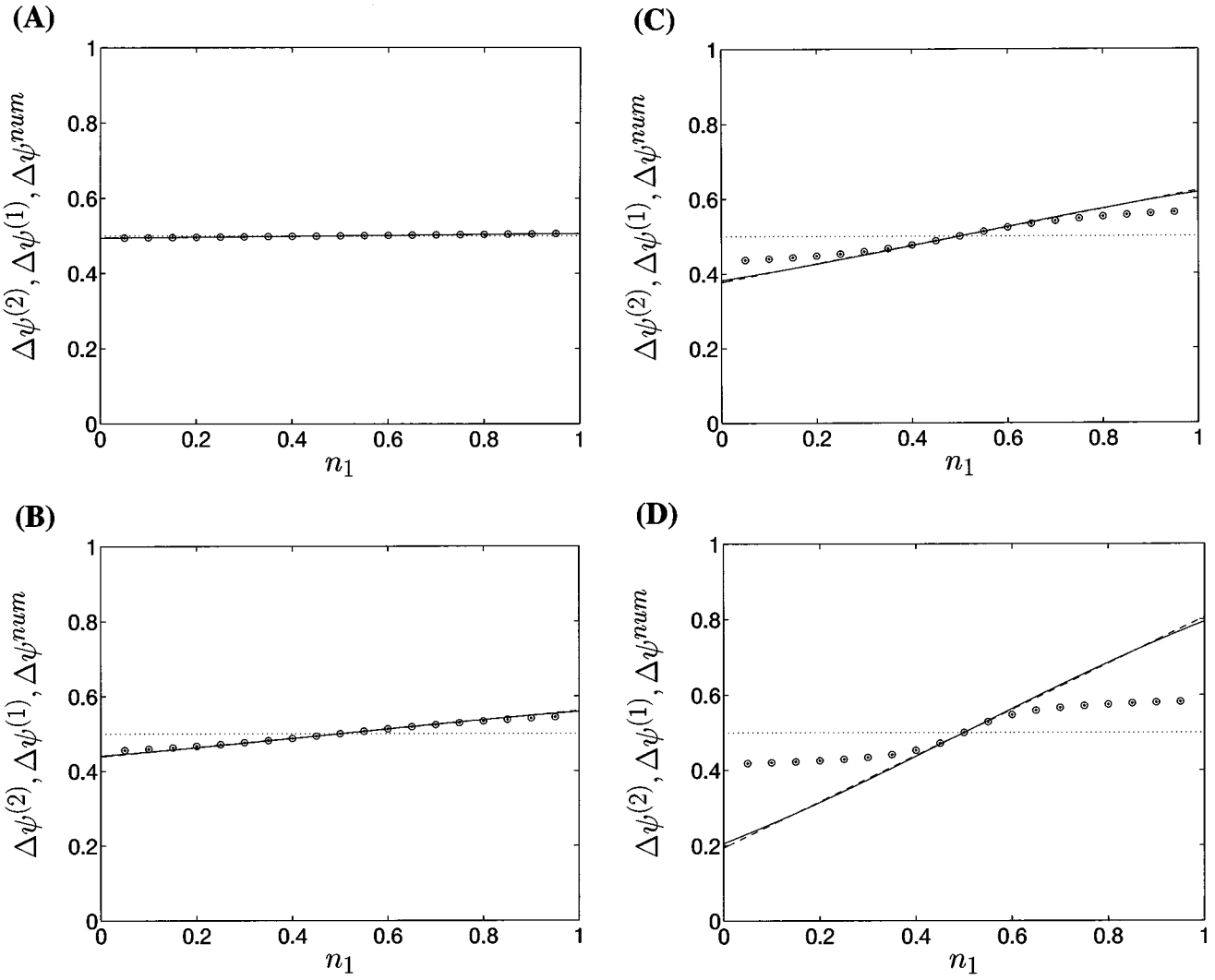

FIG. 4. *Normalized phase difference of two clusters*: Plots show $\Delta\psi^{\mathrm{num}}$ (dots, surrounded by small circles), $\Delta\psi^{(1)}$ (dashed line, covered by solid line), and $\Delta\psi^{(2)}$ (solid line) for the same model parameters as in Fig. 3 except for the values of $C_1, \ldots, C_4$: $C_1=C_3=0.01$, $C_2=C_4=-0.01$ (A) [fulfilling smallness condition (10), i.e., $|C_j| \ll \gamma = 2K_2+4K_4$], $C_1=C_3=0.1$, $C_2=C_4=-0.1$ (B), $C_1=C_3=0.2$, $C_2=C_4=-0.2$ (C), $C_1=C_3=0.5$, $C_2=C_4=-0.5$ (D).

tude R and phase Ψ of all oscillators and amplitude R_ν and phase Ψ_ν of the νth cluster, where $Re^{i\Psi}=N^{-1}\Sigma_{k=1}^{N}e^{i\psi_k}$ and $R_\nu e^{i\Psi_\nu}=N_\nu^{-1}\Sigma_{k(\nu)}e^{i\psi_k}$. Note that $0 \leqslant R \leqslant 1$ as well as $0 \leqslant R_\nu \leqslant 1$. Additionally we introduce $F=N^{-1}\Sigma_{k=1}^{N}\dot{\psi}_k$, i.e., the momentary mean frequency of all oscillators. Figures 7 and 8 show how the system approaches a frozen one-cluster state as indicated by the amplitude $R(\rightarrow 1$ for $t\rightarrow\infty)$. Figure 7 shows a transition from an unstable two-cluster state to the stable frozen state, whereas Fig. 8 shows a transition from an unstable three-cluster state (mean phase difference between neighboring clusters equals $2\pi/3$) to the stable frozen state. Note that the synchronization frequencies of the frozen state as well as the two unstable initial states totally agree with our analytically derived results [Eqs. (13), (25), (26), (28), and (29)] even though the initial states are unstable.

C. Transient behavior

For $C_j \neq 0$ cluster states of different configuration are generically associated with different synchronization frequencies. Thus for $C_j \neq 0$ transitions between different configurations give rise to transitions between different synchronization frequencies. The term synchronization frequency in the context of an unstable synchronized state denotes the oscillators' mean frequency in this particular state. Transitions of this kind may occur due to noise. However, in this article we restrict ourselves to the analysis of the deterministic dynamics of model equation (2). In future work we plan to report on the impact of noise on the model's synchronization behavior. However, in the simulations shown in Figs. 7 and 8 we already encountered transitions between different configurations occurring in our deterministic model. Let us consider what happens if a synchronized state is an unstable fixed point. Let the system start in a neighborhood of an unstable fixed point and let it be attracted by a stable synchronized state, i.e., a stable fixed point. Depending on the relationship of the synchronization frequency of the unstable and the stable synchronized state the oscillators' mean frequency F may increase (Fig. 9), decrease (Fig. 10), or remain unchanged (Fig. 11). As shown in Sec. III D for $C_1=\cdots=C_4=0$ the synchronization frequency remains unchanged as ρ and F are conserved quantities. Except for

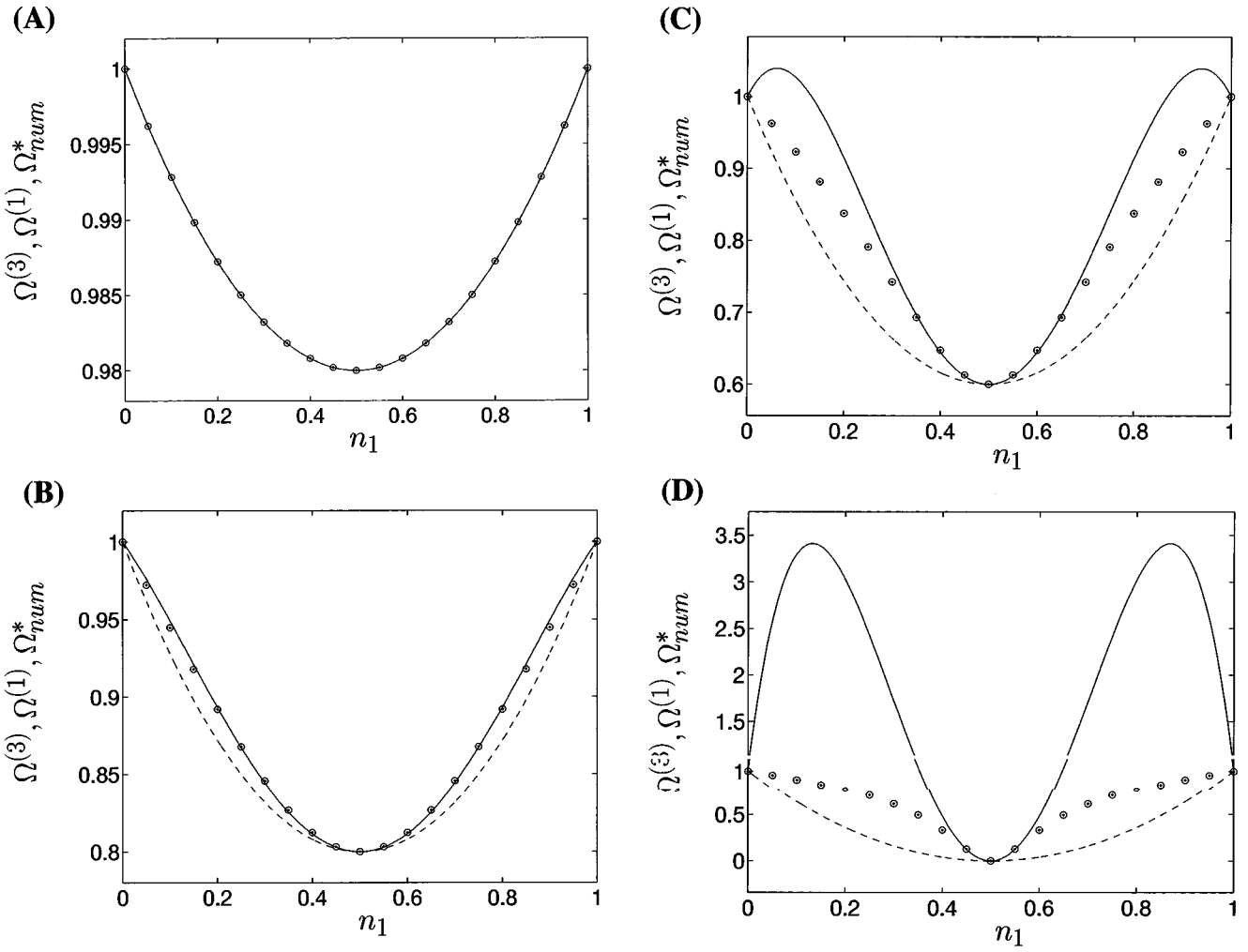

FIG. 5. *Frequency shifts of two clusters*: Plots compare analytically derived and numerically revealed frequency shifts in the synchronized states of two clusters with parameters as in Fig. 3. Ω^*_{num} (dots, surrounded by small circles), $\Omega^{(1)}$ (dashed line), and $\Omega^{(3)}$ (solid line) are determined and plotted according to the explanation in the text. Plots show frequency shifts for different values of $C_1, \ldots, C_4$: $C_1 = C_3 = -0.01$, $C_2 = C_4 = 0.01$ (A) [fulfilling smallness condition (10), i.e., $|C_j| \ll \gamma = 2K_2 + 4K_4$], $C_1 = C_3 = -0.1$, $C_2 = C_4 = 0.1$ (B), $C_1 = C_3 = -0.2$, $C_2 = C_4 = 0.2$ (C), $C_1 = C_3 = -0.5$, $C_2 = C_4 = 0.5$ (D). In order to illustrate differences between analytically derived and numerically revealed frequency shifts $\Omega^{(1)}$ and $\Omega^{(3)}$ are plotted as continuous functions of n_1 (cf. Fig. 3).

$C_1 = \cdots = C_4 = 0$ the model parameters of the simulation in Fig. 11 are the same as in Figs. 9 and 10.

Note that the synchronization frequencies of the unstable synchronized states revealed by numerical integration and shown in Figs. 9 up to 11 totally agree with the analytical results obtained in Sec. III D.

V. NEURAL CODING

In this section we sketch how model equation (2) is related to neural networks. There are different approaches for modeling the dynamics of populations of neurons, for instance, by means of networks of integrate-and-fire oscillators [27,40] and networks of limit cycle oscillators [26,28]. This article does not aim at particular details of network models. Rather we focus on dynamical phenomena which may be important from the physiological standpoint. For this reason we briefly mention how the dynamics of neurons can be approximated by limit cycle oscillators. However, we expect that synchronized states of this kind occur in networks of integrate-and-fire oscillators, too.

We take into account two types of neurons: firing and bursting neurons. The membrane potential of periodically firing neurons runs on a limit cycle [41], whereas the slow dynamics of the relaxation oscillation which generates the bursts displays a limit cycle [42,43]. For this reason we model a single neuron of both types by means of a limit cycle oscillator with time-dependent phase $\psi(t)$ and time-dependent amplitude $r(t)$. Phase and amplitude of an isolated neuron obey evolution equations which are of the form $\dot{r} = f(r, \psi)$ and $\dot{\psi} = \omega + g(r, \psi)$, where ω denotes the eigenfrequency. We are allowed to assume that a suitable transformation has been performed so that on the limit cycle $\dot{r} = 0$ holds [31,42]. Normal form theory guarantees that this assumption is fulfilled [44]. Whenever $\psi(t) = 0$ (modulo 2π), the neuron fires or bursts, depending on whether it is a firing or bursting neuron. The eigenfrequency ω models, e.g., the retinal input of a neuron in the visual cortex. The neurons' mutual excitatory and inhibitory interactions are modeled by the oscillators' mutual coupling. This way, the dynamics of a network of neurons can be approximated by a

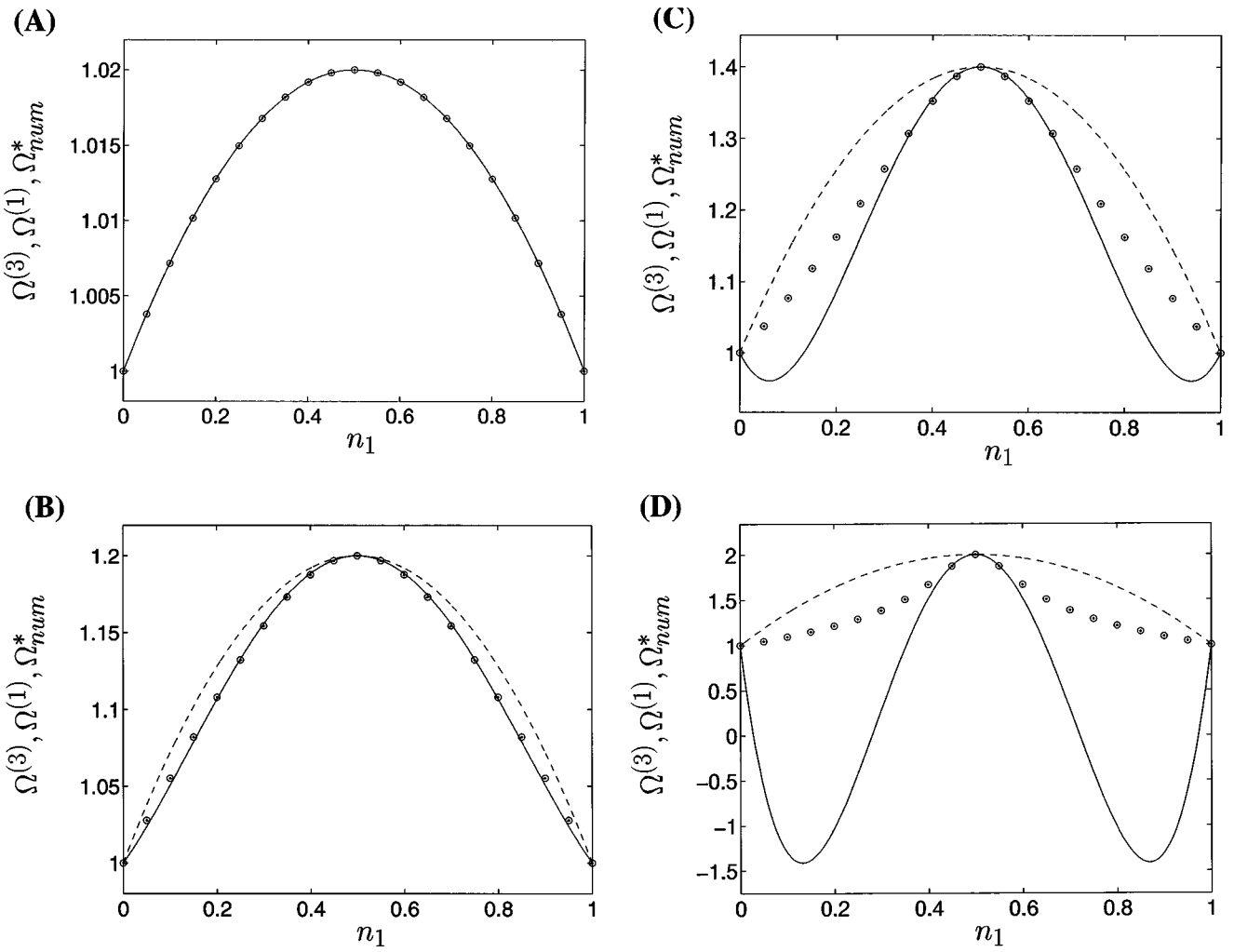

FIG. 6. *Frequency shifts of two clusters*: Plots show Ω^*_{num} (dots, surrounded by small circles), $\Omega^{(1)}$ (dashed line), and $\Omega^{(3)}$ (solid line) for the same model parameters as in Fig. 3 except for the values of $C_1, \ldots, C_4$: $C_1=C_3=0.01$, $C_2=C_4=-0.01$ (A) [fulfilling smallness condition (10), i.e., $|C_j| \ll \gamma = 2K_2+4K_4$], $C_1=C_3=0.1$, $C_2=C_4=-0.1$ (B), $C_1=C_3=0.2$, $C_2=C_4=-0.2$ (C), $C_1=C_3=0.5$, $C_2=C_4=-0.5$ (D).

population of coupled limit cycle oscillators. As explained in Sec. II populations of coupled limit cycle oscillators can approximately be described by populations of phase oscillators. Thus finally we end up with models which are of the form of Eq. (1). Note that along the lines of this phase reduction approach Hansel *et al.* derived a model equation governing the phase dynamics of two spiking Hodgkin-Huxley neurons coupled by weak excitatory interactions [45]. For further details we refer to previous studies [26,28].

Of course, the oscillators' synchronization behavior relies on the coupling Γ_{jk} [Eq. (1)]. Approximating Γ_{jk} by lowest order Fourier terms gives rise to models which typically display a one-cluster state [31]. According to previous studies (cf. [20,21]) and to our analysis due to higher order Fourier terms of the coupling Γ_{jk} a variety of additional and qualitatively different synchronization phenomena occur, for instance, one observes n-cluster states, oscillatory cluster states, and chaotic dynamics.

Thus from a theoretical point of view we expect that populations of neurons may exhibit n-cluster states, too. Based on this conjecture one may speculate about the physiological function of these cluster states. Let us, for instance, consider sensory segmentation. Augmenting the concept of von der Malsburg and Schneider [5] we might propose that all neurons, which encode local features belonging to one particular object, join into two or more phase-locked clusters. In comparison with the original concept of von der Malsburg and Schneider phase-locked clusters open up an additional effective encoding mechanism, where additional attributes of the object can be encoded by (a) the type of the cluster state (e.g., two-cluster state) and (b) the configuration of the cluster state. Moreover, a particular object might be encoded dynamically, i.e., by means of (a) transitions between different configurations, where the type of the cluster state remains the same, and (b) transitions between different types of cluster states, e.g., a transition from a two-cluster state to a three-cluster state. As a consequence of such transitions, for instance, unstable cluster states may disappear, whereas stable cluster states evolve as analyzed in Sec. IV C. On the other hand, e.g., oscillations between different unstable cluster states may occur as investigated by Hansel *et al.* [20].

According to our results transitions between different cluster states are typically associated with transitions be-

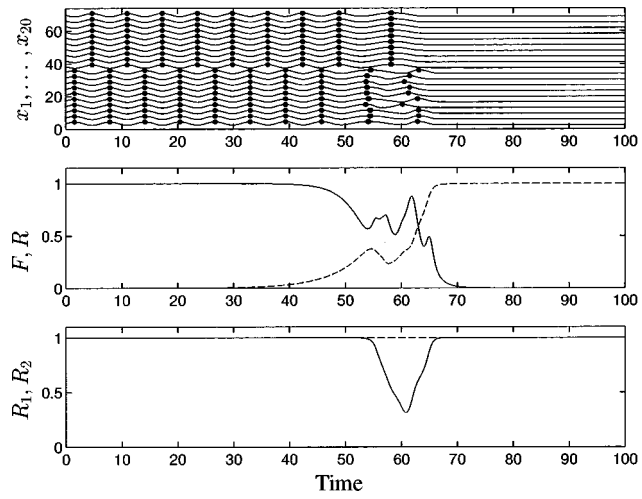

FIG. 7. *Frozen state*: Plots show transition from an unstable two-cluster state to a stable frozen one-cluster state. Numerical integration of model equation (2) for $N=20$, $K_1=0.2$, $K_2=K_3=K_4=0.01$, $C_1=C_3=0.5$, $C_2=C_4=0$. Initial phases of clusters 1 and 2 [i.e., $\psi_1(0), \ldots, \psi_{10}(0)$ and $\psi_{11}(0), \ldots, \psi_{20}(0)$] are normally distributed around 0 and π with standard deviation 0.001. Upper plot shows $x_k=\sin\psi_k+3.5k$ for all oscillators ($k=1, \ldots, 20$). Local maxima of $x_1, \ldots, x_{20}$ are indicated by black dots in order to illustrate the synchronization configuration. Middle plot shows mean frequency of all oscillators F (solid line) and amplitude of all oscillators R (dashed line). Lower plot displays amplitudes of cluster 1 (R_1, solid line) and cluster 2 (R_2, dashed line).

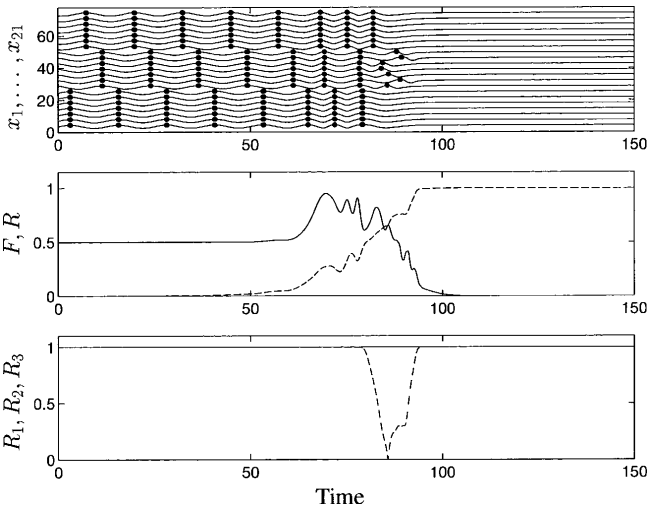

FIG. 8. *Frozen state*: Unstable three-cluster state vanishes, and stable frozen one-cluster state evolves. Numerical integration of model equation (2) for $N=21$, $K_1=0.2$, $K_2=K_3=K_4=0.01$, $C_1=C_3=0.5$, $C_2=C_4=0$. Initial phases of clusters 1, 2, 3 [i.e., $\psi_1(0), \ldots, \psi_7(0)$, $\psi_8(0), \ldots, \psi_{14}(0)$, $\psi_{15}(0), \ldots, \psi_{21}(0)$] are normally distributed around 0, $2\pi/3$, $4\pi/3$ with standard deviation 0.001. Upper plot shows $x_k=\sin\psi_k+3.5k$ for all oscillators ($k=1, \ldots, 21$). Local maxima of $x_1, \ldots, x_{21}$ are indicated by black dots. Middle plot shows mean frequency of all oscillators F (solid line) and amplitude of all oscillators R (dashed line). Lower plot displays amplitudes of cluster 1 (R_1, solid line), cluster 2 (R_2, dashed line), and cluster 3 (R_3, dotted line, covered by solid line).

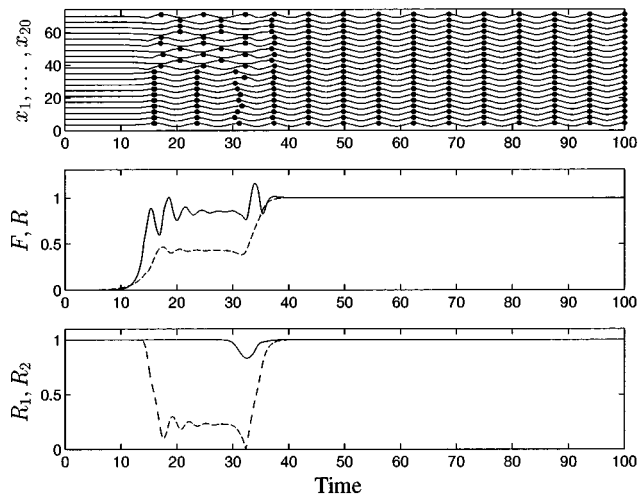

FIG. 9. *Transient behavior*: Unstable frozen two-cluster state vanishes, and stable one-cluster state evolves. Numerical integration of model equation (2) for $N=20$, $K_1=0.5$, $K_2=K_3=K_4=0.01$, $C_1=0$, $C_3=-1$, $C_2=C_4=0.5$. Initial phases of clusters 1 and 2 [i.e., $\psi_1(0), \ldots, \psi_{10}(0)$ and $\psi_{11}(0), \ldots, \psi_{20}(0)$] are normally distributed around 0 and π with standard deviation 0.001. Upper plot shows $x_k=\sin\psi_k+3.5k$ for all oscillators ($k=1, \ldots, 20$). Local maxima of $x_1, \ldots, x_{20}$ are indicated by black dots. Middle plot shows mean frequency of all oscillators F (solid line) and amplitude of all oscillators R (dashed line). Lower plot displays amplitudes of cluster 1 (R_1, solid line), cluster 2 (R_2, dashed line), and cluster 3 (R_3, dotted line, covered by solid line).

tween different synchronization frequencies. It is difficult or even impossible to detect dynamical phenomena of this kind by means of linear correlation techniques. Whether phase-locked clusters play an important role in neural coding can only be decided experimentally. Of course, this can only be done if the experimentalists are provided with appropriate data analysis tools.

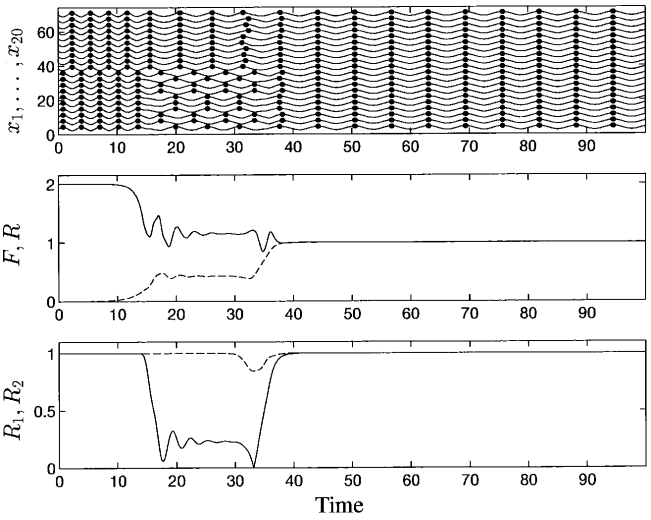

FIG. 10. *Transient behavior*: Transition from an unstable two-cluster state to a stable one-cluster state. Numerical integration and model parameters as in Fig. 9 except for $C_1=0$, $C_3=1$, $C_2=C_4=-0.5$. The same format as in Fig. 9 is used.

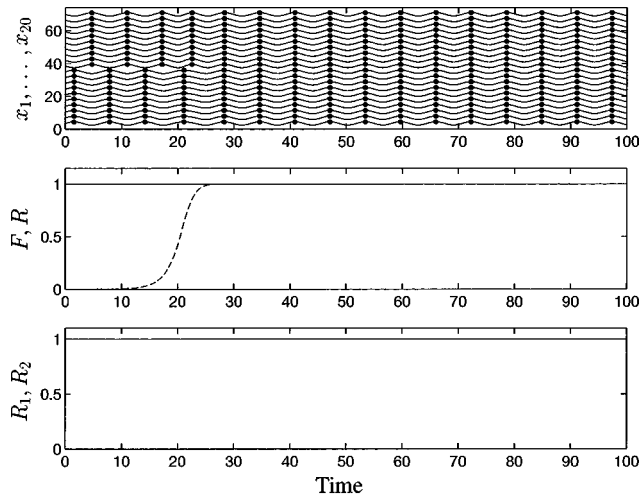

FIG. 11. *Transient behavior*: Transition from an unstable two-cluster state to a stable one-cluster state. Parameters as in Fig. 9 except for $C_1=C_2=C_3=C_4=0$. The same format as in Fig. 9. Note that F is a conserved quantity.

The synchronization behavior of model equation (2) is not only interesting in the context of neural coding. This model may also be a starting point for the analysis of other dynamical phenomena well known from neurophysiology. We briefly mention two examples.

(a) Transient phenomena associated with changes of the synchronization behavior abound in neurophysiology. For instance, one may consider transient changes of the electromyographically recorded burst pattern induced by single rapid isometric finger extensions [46].

(b) The second example refers to bimanual movement coordination. Haken, Kelso, and Bunz developed a paradigmatic macroscopic model for phase transitions in human hand movements [47]. The latter describes the oscillatory dynamics of the two index fingers: An increase of the movement frequency gives rise to a transition from an antiphase mode into an in-phase mode. Equation (2) can be used in order to develop a mesoscopic version of the Haken-Kelso-Bunz model describing the activity of populations of neurons located in the left and right motor cortex: For simplicity we set $K_3=K_4=C_j=0$. Both K_1 and K_2 depend on the movement frequency, where with increasing movement frequency K_1 increases and K_2 decreases. This causes a transition from a two-cluster state to a one-cluster state. In the two-cluster state the two populations which are located in different motor cortices fire in antiphase, whereas in the one-cluster state both neuronal populations fire in unison.

VI. DISCUSSION

In this study we investigated phase-locked synchronized states which may be important from the physiological point of view, e.g., in the context of neural coding. The starting point of our analysis is Eq. (1), the famous model of continuously interacting phase oscillators [30,31]. In former studies the 2π-periodic coupling Γ_{jk} was typically approximated by lowest order Fourier modes (see, e.g., [31]). For instance, the interactions of globally coupled phase oscillators were modeled by $\Gamma_{jk}(\psi_j-\psi_k)=\Gamma(\psi_j-\psi_k)=KN^{-1}\sin(\psi_j-\psi_k)$, where K is the coupling strength, and N is the number of oscillators. If the coupling is strong enough as compared with the spread of the eigenfrequencies, the oscillators are joined into one giant cluster [31].

Obviously the coupling decisively determines the synchronization behavior. Thus even in the case of globally coupled oscillators one might expect that for different coupling Γ qualitatively different synchronized states occur. For this reason in the present article we investigated a population of globally coupled phase oscillators, where in contrast to former studies the coupling was approximated by Fourier modes up to fourth order [cf. Eq. (2)]. According to our results this model displays a rich synchronization behavior. Aside from in-phase synchronization (one-cluster state) we encounter qualitatively different phase-locked states: two-cluster states, three-cluster states, and four-cluster states as illustrated in Fig. 1. The model parameters and the initial conditions determine whether all oscillators form one giant cluster or whether they break into two, three, or four phase-locked clusters of arbitrary size. Within one cluster the phase difference between any two oscillators vanishes or is small as compared with the phase difference between different clusters (cf. Fig. 1).

The synchronized states analyzed in this study are phase-locked states in which all oscillators run at the same frequency, i.e., $\dot{\psi}_j=\Omega^*$ for $j=1,\ldots,N$. Lower order shifts of the synchronization frequency depend on the configuration, i.e., the number of oscillators within each cluster, whereas higher order shifts additionally depend on the eigenfrequency distribution (cf. Fig. 2). For suitably chosen and fixed model parameters the synchronization frequency vanishes for a particular configuration. We denote synchronized states with vanishing synchronization frequency as frozen states. If the latter are unstable fixed points we typically encounter transients during which an initially vanishing synchronization frequency increases (cf. Fig. 9). Lower order shifts and higher order shifts of the mutual phase differences depend on the configuration as well as on the eigenfrequency distribution.

If all oscillators have the same eigenfrequency ($\omega_j=\Omega$), every configuration is associated with a multiplicity of attractors according to Eq. (33). For $C_j\neq 0$ [cf. Eq. (2)] each configuration generically corresponds to a particular synchronization frequency. Thus we encounter a degeneracy of the synchronized states as far as the synchronization frequency is concerned (cf. Fig. 2). As illustrated in Fig. 2 this degeneracy vanishes due to randomly distributed eigenfrequencies.

Both frequency shifts and phase shifts were explicitly determined by means of a combination of center manifold theorem and a nonlinear renormalization procedure. Thereby we had to assume that the spread of the eigenfrequencies and some of the model parameters are small in comparison with the synchronizing coupling constants [cf. condition (10)]. For larger values of the spread and of the model parameters we checked our results numerically. Our approach can easily be applied in the case of randomly distributed coupling coefficients, too. To this end for the coupling constants between jth and kth oscillator we set $K_{jk}=K_m+\varepsilon\widetilde{K}_{jk}$ and $C_{jk}=C_m+\varepsilon\widetilde{C}_{jk}$, where the jth oscillator is in the mth clus-

ter. $\{K_{jk}\}$ and $\{C_{jk}\}$ give rise to additional terms of phase and frequency shifts.

In several previous studies the cluster states under consideration were not essentially phase-locked states [17–19]. As yet the latter were addressed by only a few studies.

Okuda analyzed globally coupled phase oscillators, where the coupling contained higher harmonics, and the coupling coefficients were attractive as well as repulsive [21]. His investigation revealed a rich dynamical behavior, for instance, aside from in-phase states he observed antiphase states, oscillating cluster states, and chaotic long transients. Okuda focused on ''symmetric'' cluster states where each cluster contains the same number of oscillators. On the other hand, in his model all oscillators had the same eigenfrequency ($\omega_j=\Omega$). Hence he was not able to study how frequency shifts depend on the cluster state configuration and on the oscillators' detuning.

Phase-locked cluster states in a network of globally coupled oscillators were also studied by Hansel *et al.* [20]. The coupling in their model contained Fourier modes of first and second order. Due to the choice of model parameters they observed three typical types of dynamics: a one-cluster state, a totally incoherent state, and a pair of unstable two-cluster states connected by a homoclinic orbit. In the last regime adding noise gives rise to oscillations between the two two-cluster states. The oscillators in their model had uniform eigenfrequencies ($\omega_j=\Omega$), too. For this reason also this study was not devoted to the influence of eigenfrequency detuning and configuration on the synchronization frequency of stable n-cluster states.

Antiphase synchronization caused by repulsive coupling was investigated in a model for synchronized oscillations in the visual cortex by Tass and Haken [28,33]. In their model the synchronized state corresponds to one attractor (modulo 2π). In particular, the configuration only depends on the distribution of repulsive and attractive coupling. Moreover, in this model we do not encounter a multiplicity of attractors.

Models of globally coupled oscillators are widely used, for instance, in the context of multimode lasers [48], Josephson junction arrays [49], and biological populations, such as fireflies [50] and crickets [51]. As discussed in the former section our results are additionally interesting from the standpoint of neurophysiology.

(1) Model equation (2) can be augmented to become a mesoscopic version of the Haken-Kelso-Bunz model for bimanual coordination [47].

(2) Transient phenomena associated with changes of the synchronization behavior are frequently observed in electromyographic studies (cf. [46]).

(3) In contrast to coding by synchrony the phase-locked cluster states mentioned above open up additional coding facilities. For instance, let us consider sensory segmentation: An object as a whole could be encoded by means of neurons joined into a phase-locked cluster state, whereas additional information could be encoded by means of the configuration of this particular cluster state.

The relevancy of the above mentioned cluster states to neural coding and other neurophysiological phenomena can only be checked experimentally. To this end experimentalists have to be able to detect (a) the cluster states and (b) transitions between different cluster states. Obviously this is a challenge for nonlinear data analysis.

Let us finally mention that from the neurophysiological as well as theoretical point of view it is important to investigate the role the noise in the synchronization behavior of Eq. (2) plays. For instance, due to the multiplicity of attractors, in particular, in the thermodynamic limit ($N\gg 1$) one might expect similar effects as revealed in the context of attractor crowding [14]. Our results concerning the influence of noise on the synchronization behavior of our model will be presented in a forthcoming article.

ACKNOWLEDGMENTS

I am grateful to Hans-Joachim Freund, Harald Hefter, and Arne Wunderlin for our fruitful discussions. This study was supported by the Deutsche Forschungsgemeinschaft SFB 194 (A5).

APPENDIX A: TWO CLUSTERS

Frequency shifts of higher order are

$$\delta_{(3)}=d_1V+d_2(n_1^2V_1+n_2^2V_2)+d_3(n_2-n_1)n_1\Lambda_1, \tag{A1}$$

$$\delta_{(3)}^{\dagger}=d_4(n_1-n_2)^2n_1n_2, \tag{A2}$$

where V, V_j, and Λ_1 are defined in Sec. II, and

$$d_1=\frac{C_1-8C_2+9C_3-32C_4}{8\varepsilon^2(K_2+2K_4)^2}, \quad d_2=-\frac{3(C_1+9C_3)}{8\varepsilon^2(K_2+2K_4)^2}, \tag{A3}$$

$$d_3=\frac{(C_1+C_3)(C_1-8C_2+9C_3-32C_4)}{2\varepsilon(K_2+2K_4)^2}, \tag{A4}$$

$$d_4=\frac{(C_1+C_3)^2(C_1-8C_2+9C_3-32C_4)}{2(K_2+2K_4)^2}. \tag{A5}$$

Higher order terms of the phase shift in the synchronized state read

$$\chi_j=\frac{1}{2K_2+4K_4}\eta_j+\varepsilon\frac{K_1+3K_3}{4(K_2+2K_4)^2}\times[(n_\nu-n_\mu)\eta_j+n_\nu\Lambda_\nu-n_\mu\Lambda_\mu], \tag{A6}$$

$$\chi_j^{\dagger}=\varepsilon\frac{C_1+C_3}{2K_2+4K_4}[n_\mu-n_\nu+(n_\nu-n_\mu)^2]+\varepsilon^2\frac{(C_1+C_3)(K_1+3K_3)}{2(K_2+2K_4)^2}[n_\nu(n_\mu-n_\nu)+(n_\nu-n_\mu)^3]+O(\|\mathbf{x}_c\|^3) \tag{A7}$$

for the jth oscillator in the νth cluster, $\mu\neq\nu$ (i.e., $\nu=1,\mu=2$ or $\nu=2,\mu=1$), Λ_ν as introduced in Sec. II.

APPENDIX B: THREE CLUSTERS

For the jth oscillator in the νth cluster we obtain

$$H_j(\mathbf{x}_c)=\frac{\delta_{(2)}\varepsilon^2}{3K_3}+\{f_j(n_{\nu+}+n_{\nu-}-2n_\nu)-g_j(n_{\nu+}-n_{\nu-})\}\times\varepsilon\eta_j+f_j\varepsilon(2n_\nu\Lambda_\nu-n_{\nu+}\Lambda_{\nu+}-n_{\nu-}\Lambda_{\nu-})+g_j\varepsilon(n_{\nu+}\Lambda_{\nu+}-n_{\nu-}\Lambda_{\nu-})+O(\|\mathbf{x}_c\|^3), \tag{B1}$$

$$H_j^\dagger(\mathbf{x}_c)=\frac{\delta_{(2)}^\dagger\varepsilon^2}{3K_3}+\{f_j(n_{\nu+}+n_{\nu-}-2n_\nu)-g_j(n_{\nu+}-n_{\nu-})\}\times\varepsilon\eta_j^\dagger+f_j\varepsilon(2n_\nu\eta_{k(\nu)}^\dagger-n_{\nu+}\eta_{k(\nu+)}^\dagger-n_{\nu-}\eta_{k(\nu-)}^\dagger)+g_j\varepsilon(n_{\nu+}\eta_{k(\nu+)}^\dagger-n_{\nu-}\eta_{k(\nu-)}^\dagger)+O(\|\mathbf{x}_c\|^3), \tag{B2}$$

$f_j=(K_1+2K_2+4K_4)/(18K_3^2)$, $g_j=(C_1-2C_2+4C_4)/(6\sqrt{3}K_3^2)$, and $n_{\nu+}=n_{[\nu+1]_3}$, $n_{\nu-}=n_{[\nu-1]_3}$, where $[k]_m=[k]_{\mathrm{mod}\,m}$ (e.g., $[5]_3=2$). By $\eta_{k(\nu)}^\dagger,\eta_{k(\nu+)}^\dagger,\eta_{k(\nu-)}^\dagger$ we denote $\eta_k^\dagger$, where the kth oscillator is in cluster ν, $[\nu+1]_3$, $[\nu-1]_3$. The shifts of the eigenfrequencies read

$$\eta_j^\dagger=\frac{\varepsilon\sqrt{3}}{2}(n_{[\nu+1]_3}-n_{[\nu-1]_3})(K_1-K_2+K_4)+\varepsilon(C_1+C_2+C_4)\frac{1}{2}\left\{\sum_{k=1}^{3}(n_k-n_{[k+1]_3})^2+n_{[k-1]_3}+n_{[k+1]_3}-2n_k\right\} \tag{B3}$$

for the jth oscillator in the νth cluster. Terms of second order of the synchronization frequency are

$$\delta_{(2)}=\frac{C_1-2C_2+4C_4}{\sqrt{3}\varepsilon K_3}\sum_{k=1}^{3}(n_{[k+1]_3}-n_{[k-1]_3})n_k\Lambda_k, \tag{B4}$$

with Λ_k from Sec. II, and

$$\delta_{(2)}^\dagger=\frac{C_1-2C_2+4C_4}{K_3}\left[\frac{1}{2}(K_1-K_2+K_4)\left(\sum_{k=1}^{3}n_kn_{[k+1]_3}-9n_1n_2n_3\right)+\frac{1}{2\sqrt{3}}(C_1+C_2+C_4)\times\sum_{k=1}^{3}(n_k-n_{[k+1]_3})^2\right]. \tag{B5}$$

APPENDIX C: FOUR CLUSTERS

The shifts of the eigenfrequencies are

$$\eta_j^\dagger=\varepsilon(K_1-K_3)(n_{[\nu+1]_4}-n_{[\nu-1]_4})+\varepsilon C_2\{(n_1+n_3-n_2-n_4)^2+n_{[\nu+1]_4}+n_{[\nu-1]_4}-n_\nu-n_{[\nu+2]_4}\}+\varepsilon(C_1+C_3)\times[(n_1-n_3)^2+(n_2-n_4)^2+n_{[\nu+2]_4}-n_\nu], \tag{C1}$$

for the jth oscillator in the νth cluster. Higher order frequency shifts in the synchronized state read

$$\delta_{(2)}=\frac{C_1-3C_3}{2\varepsilon K_4}\{(n_2-n_4)(n_1\Lambda_1-n_3\Lambda_3)+(n_3-n_1)(n_2\Lambda_2-n_4\Lambda_4)\}, \tag{C2}$$

with Λ_k as introduced in Sec. II, and

$$\delta_{(2)}^\dagger=\frac{C_1-3C_3}{2K_4}(D_1+D_2), \tag{C3}$$

where

$$D_1=(K_1-K_3)[(n_1+n_3)(n_2-n_4)^2+(n_2+n_4)(n_1-n_3)^2], \tag{C4}$$

$$D_2=(C_1+2C_2+C_3)(n_2+n_4-n_1-n_3)(n_1-n_3)(n_2-n_4). \tag{C5}$$

For the jth oscillator of the νth cluster we get higher order phase shifts

$$H_j(\mathbf{x}_c)=\frac{\delta_{(2)}\varepsilon^2}{4K_4}+\left\{\frac{K_1+3K_3}{64K_4^2}(n_{\nu++}-n_\nu)+\frac{K_2}{8K_4^2}(n_{\nu+}+n_{\nu-}-n_\nu-n_{\nu++})-\frac{C_1-3C_3}{64K_4^2}(n_{\nu+}-n_{\nu-})\right\}\varepsilon\eta_j+\frac{K_1+3K_3}{64K_4^2}\varepsilon(n_\nu\Lambda_\nu+n_{\nu++}\Lambda_{\nu++})+\frac{K_2}{8K_4^2}\varepsilon\left(n_{\nu++}\Lambda_{\nu++}-\sum_{\substack{\mu\\ \mu\neq\nu++}}n_\mu\Lambda_\mu\right)+\frac{C_1-3C_3}{64K_4^2}\varepsilon(n_{\nu+}\Lambda_{\nu+}-n_{\nu-}\Lambda_{\nu-})+O(\|\mathbf{x}_c\|^3), \tag{C6}$$

$$H_j^\dagger(\mathbf{x}_c)=\frac{\delta_{(2)}^\dagger\varepsilon^2}{4K_4}+\left\{\frac{K_1+3K_3}{64K_4^2}(n_{\nu++}-n_\nu)+\frac{K_2}{8K_4^2}(n_{\nu+}+n_{\nu-}-n_\nu-n_{\nu++})-\frac{C_1-3C_3}{64K_4^2}(n_{\nu+}-n_{\nu-})\right\}\varepsilon\eta_j^\dagger+\frac{K_1+3K_3}{64K_4^2}\varepsilon(n_\nu\eta_{k(\nu)}^\dagger+n_{\nu++}\eta_{k(\nu++)}^\dagger)+\frac{K_2}{8K_4^2}\varepsilon\left(n_{\nu++}\eta_{k(\nu++)}^\dagger-\sum_{\substack{\mu\\ \mu\neq\nu++}}n_\mu\eta_{k(\mu)}^\dagger\right)+\frac{C_1-3C_3}{64K_4^2}\varepsilon(n_{\nu+}\eta_{k(\nu+)}^\dagger-n_{\nu-}\eta_{k(\nu-)}^\dagger)+O(\|\mathbf{x}_c\|^3), \tag{C7}$$

and $n_{\nu+}=n_{[\nu+1]_4}$, $n_{\nu++}=n_{[\nu+2]_4}$, $n_{\nu-}=n_{[\nu-1]_4}$. Analogously $\eta_{k(\nu)}^\dagger$, $\eta_{k(\nu+)}^\dagger$, $\eta_{k(\nu++)}^\dagger$, $\eta_{k(\nu-)}^\dagger$ denote $\eta_k^\dagger$, with k in cluster ν, $[\nu+1]_4$, $[\nu+2]_4$, $[\nu-1]_4$.

[1] D. Marr, Philos. Trans. R. Soc. London, Ser. B **275**, 483 (1976); A. Treisman, in *Handbook of Perception and Human Performances*, edited by K. Boff, L. Kaufman, and I. Thomas (Wiley, New York, 1986), pp. 1–70; V. S. Ramachandran, Nature (London) **331**, 163 (1988); B. Julesz, Rev. Mod. Phys. **63**, 735 (1991).

[2] W. Singer, Concepts Neurosci. **1**, 1 (1989).

[3] D. H. Hubel and T. N. Wiesel, J. Physiol. (London) **148**, 574 (1959).

[4] D. O. Hebb, *Organization of Behavior* (Wiley, New York, 1949); P. M. Milner, Psychol. Rev. **86**, 521 (1974); M. Abeles, *Local Cortical Circuits. An Elektrophysiological Study* (Springer, Berlin, 1982); F. Crick, Proc. Natl. Acad. Sci. USA **81**, 4586 (1984); C. von der Malsburg, in *Brain Theory*, edited by G. Palm and A. Aertsen (Springer, Berlin, 1986), pp. 161–176; H. Shimizu, Y. Yamaguchi, I. Tsuda, and M. Yano, in *Complex Systems—Operational Approaches*, edited by H. Haken (Springer, Berlin, 1986), pp. 225–240; F. H. C. Crick and C. Koch, Semin. Neurosci. **2**, 263 (1990).

[5] C. von der Malsburg and W. Schneider, Biol. Cybern. **54**, 29 (1986); see also C. von der Malsburg, Max-Planck-Institute for Biophysical Chemistry, Internal Report No. 81-2, 1981 (unpublished).

[6] W. J. Freeman, *Mass Action in the Nervous System* (Academic Press, New York, 1975).

[7] C. M. Gray and W. Singer, Soc. Neurosci. **13**, 404 (1987).

[8] R. Eckhorn, R. Bauer, W. Jordan, M. Brosch, W. Kruse, M. Munk, and H. J. Reitboeck, Biol. Cybern. **60**, 121 (1988).

[9] S. Neuenschwander and F. J. Varela, Soc. Neurosci. Abstr. **16**, 47 (1990).

[10] M. S. Livingstone, Soc. Neurosci. Abstr. **17**, 73 (1991); A. Kreiter and W. Singer, Eur. J. Neurosci. **4**, 369 (1992); V. N. Murthy and E. E. Fetz, Proc. Natl. Acad. Sci. USA **89**, 5670 (1992); R. Eckhorn, A. Frien, R. Bauer, T. Woelbern, and H. Kehr, NeuroReport **4**, 243 (1993).

[11] D. H. Hubel and T. N. Wiesel, J. Physiol. (London) **160**, 106 (1962); **165**, 559 (1963).

[12] C. M. Gray and W. Singer, Proc. Natl. Acad. Sci. USA **86**, 1698 (1989); R. Eckhorn and H. J. Reitboeck, in *Synergetics of Cognition*, edited by H. Haken and M. Stadler (Springer, Berlin, 1990), pp. 99–111; W. Singer, Annu. Rev. Physiol. **55**, 349 (1993); W. Singer and C. M. Gray, Annu. Rev. Neurosci. **18**, 555 (1995).

[13] S. Nichols and K. Wiesenfeld, Phys. Rev. A **45**, 8430 (1992); S. H. Strogatz and R. Mirollo, Phys. Rev. E **47**, 220 (1993); J. W. Swift, S. H. Strogatz, and K. Wiesenfeld, Physica D **55**, 239 (1992).

[14] K. Wiesenfeld and P. Hadley, Phys. Rev. Lett. **62**, 1335 (1989).

[15] G. B. Ermentrout and N. Kopell, SIAM (Soc. Ind. Appl. Math.) J. Math. Anal. **15**, 215 (1984); G. B. Ermentrout and W. C. Troy, SIAM (Soc. Ind. Appl. Math.) J. Appl. Math. **46**, 359 (1986).

[16] A. T. Winfree, *The Geometry of Biological Time* (Springer, Berlin, 1980).

[17] H. Sakaguchi, S. Shinomoto, and Y. Kuramoto, Prog. Theor. Phys. **77**, 1005 (1987); **79**, 1069 (1988); S. H. Strogatz and R. E. Mirollo, Physica D **31**, 143 (1988); J. Phys. A **21**, L699 (1988).

[18] D. Golomb, D. Hansel, B. Shraiman, and H. Sompolinsky, Phys. Rev. A **45**, 3516 (1992).

[19] V. Hakim and W. Rappel, Phys. Rev. A **46**, R7347 (1992); N. Nakagawa and Y. Kuramoto, Prog. Theor. Phys. **89**, 313 (1993).

[20] D. Hansel, G. Mato, and C. Meunier, Phys. Rev. E **48**, 3470 (1993).

[21] K. Okuda, Physica D **63**, 424 (1993).

[22] S. K. Han, C. Kurrer, and Y. Kuramoto, Phys. Rev. Lett. **75**, 3190 (1995).

[23] A. S. Pikovsky, K. Rateitschak, and J. Kurths, Z. Phys. B **95**, 541 (1994).

[24] K. Wiesenfeld and P. Hadley, Phys. Rev. Lett. **62**, 1335 (1989); A. S. Pikovsky, M. G. Rosenblum, and J. Kurths, Europhys. Lett. **34**, 165 (1996).

[25] P. C. Matthews and S. H. Strogatz, Phys. Rev. Lett. **65**, 1701 (1990).

[26] H. G. Schuster and P. Wagner, Biol. Cybern. **64**, 77 (1990); **64**, 83 (1990); H. Sompolinsky, D. Golomb, and D. Kleinfeld, Phys. Rev. A **43**, 6990 (1991).

[27] S. Grossberg and D. Somers, Neural Networks **4**, 453 (1991); T. Chawanya, T. Aoyagi, I. Nishikawa, K. Okuda, and Y. Kuramoto, Biol. Cybern. **68**, 483 (1993); T. B. Schillen and P. König, *ibid.* **70**, 397 (1994).

[28] P. Tass and H. Haken, Biol. Cybern. **74**, 31 (1996).

[29] M. H. J. Munk, P. R. Roelfsema, P. König, A. K. Engel, and W. Singer, Science **272**, 271 (1996).

[30] A. T. Winfree, J. Theor. Biol. **16**, 15 (1967); see also Ref. [16]; G. B. Ermentrout and J. Rinzel, J. Math. Biol. **11**, 269 (1981).

[31] Y. Kuramoto, *Chemical Oscillations, Waves, and Turbulence* (Springer, Berlin, 1984).

[32] H. Daido, Phys. Rev. Lett. **73**, 760 (1994); Physica D **91**, 24 (1996); J. D. Crawford, Phys. Rev. Lett. **74**, 4341 (1995).

[33] P. Tass and H. Haken, Z. Phys. B **100**, 303 (1996).

[34] V. Pliss, Izv. Akad. Nauk. SSSR Math. Ser. **28**, 1297 (1964); A. Kelley, J. Diff. Equ. **3**, 546 (1967).

[35] H. Haken, *Synergetics. An Introduction* (Springer, Berlin, 1977).

[36] H. Haken, *Advanced Synergetics* (Springer, Berlin, 1983).

[37] P. Tass, Z. Phys. B **99**, 111 (1995).

[38] M. W. Hirsch and S. Smale, *Differential Equations, Dynamical Systems, and Linear Algebra* (Academic Press, San Diego, 1974).

[39] Y. Aizawa, Prog. Theor. Phys. **56**, 703 (1976); Y. Yamaguchi and H. Shimizu, Physica D **11**, 212 (1984); M. Shiino and M. Frankowicz, Phys. Lett. A **136**, 103 (1989).

[40] R. E. Mirollo and S. H. Strogatz, SIAM (Soc. Ind. Appl. Math.) J. Appl. Math. **50**, 1645 (1990).

[41] A. L. Hodgkin and A. F. Huxley, J. Physiol. (London) **117**, 500 (1952); R. FitzHugh, Biophys. J. **1**, 445 (1961); J. S. Nagumo, S. Arimoto, and S. Yoshizawa, Proc. IRE **50**, 2061 (1962).

[42] J. D. Murray, *Mathematical Biology* (Springer, Berlin, 1990).

[43] R. E. Plant, J. Math. Biol. **11**, 15 (1981).

[44] C. Elphik, E. Tirapegui, M. Brachet, P. Coullet, and G. Iooss, Physica D **29**, 95 (1987).

[45] D. Hansel, G. Mato, and C. Meunier, Europhys. Lett. **23**, 367 (1993).

[46] H. Hefter, O. W. Witte, K. Reiners, E. Niedermeyer, and H.-J. Freund, Electromyogr. Clin. Neurophysiol. **34**, 95 (1995).

[47] H. Haken, J. A. S. Kelso, and H. Bunz, Biol. Cybern. **51**, 347 (1985).
[48] K. Wiesenfeld, C. Bracikowski, G. James, and R. Roy, Phys. Rev. Lett. **65**, 1749 (1990); K. Otsuka, *ibid.* **67**, 1090 (1991).
[49] P. Hadley, M. R. Beasley, and K. Wiesenfeld, Phys. Rev. B **38**, 8712 (1988); K. Y. Tsang and K. Wiesenfeld, Appl. Phys. Lett. **56**, 495 (1990).
[50] J. Buck and E. Buck, Sci. Am. **234**, 74 (1976).
[51] T. J. Walker, Science **166**, 891 (1969).